MIT Libraries | DSpace@MIT

MIT Open Access Articles

Modelling of the EAST lower-hybrid current drive experiment using GENRAY/CQL3D and TORLH/CQL3D

The MIT Faculty has made this article openly available. ***Please share*** how this access benefits you. Your story matters.

Citation: Yang, C et al. "Modelling of the EAST Lower-Hybrid Current Drive Experiment Using GENRAY/CQL3D and TORLH/CQL3D." Plasma Physics and Controlled Fusion 56, 12 (October 2014): 125003 © 2014 IOP Publishing Ltd

As Published: http://dx.doi.org/10.1088/0741-3335/56/12/125003

Publisher: IOP Publishing

Persistent URL: http://hdl.handle.net/1721.1/113073

Version: Author's final manuscript: final author's manuscript post peer review, without publisher's formatting or copy editing

Terms of Use: Article is made available in accordance with the publisher's policy and may be subject to US copyright law. Please refer to the publisher's site for terms of use.

Massachusetts Institute of Technology

Modelling of the EAST lower-hybrid current drive experiment using GENRAY/CQL3D and TORLH/CQL3D

C. Yang[a], P. T. Bonoli[b], J. C. Wright[b], B. Ding[a], R. Parker[b], S. Shiraiwa[b] and M. H. Li[a]

[a] Chinese Academy of Sciences - Hefei Institutes of Physical Sciences, Institute of Plasma Physics, Hefei, China

[b]Plasma Science and Fusion Center, MIT, Cambridge, MA (USA)

Abstract: The coupled GENRAY-CQL3D code has been used to do systematic ray-tracing and Fokker-Planck analysis for EAST Lower Hybrid wave Current Drive (LHCD) experiments. Despite being in the weak absorption regime, the experimental level of LH current drive is successfully simulated, by taking into account the variations in the parallel wavenumber due to the toroidal effect. The effect of radial transport of the fast LH electrons in EAST has also been studied, which shows that a modest amount of radial transport diffusion can redistribute the fast LH current significantly. Taking advantage of the new capability in GENRAY, the actual Scrape Off Layer (SOL) model with magnetic field, density, temperature, and geometry is included in the simulation for both the lower and the higher density cases, so that the collisional losses of Lower Hybrid Wave (LHW) power in the SOL has been accounted for, which together with fast electron losses can reproduce the LHCD experimental observations in different discharges of EAST. We have also analyzed EAST discharges where there is a significant ohmic contribution to the total current, and good agreement with experiment in terms of total current has been obtained. Also, the full-wave code TORLH has been used for the simulation of the LH physics in the EAST, including full-wave effects such as diffraction and focusing which may also play an important role in bridging the spectral gap. The comparisons between the GENRAY and the TORLH codes are done for both the Maxwellian and the quasi-linear electron Landau damping cases. These simulations represent an important addition

to the validation studies of the GENRAY-CQL3D and TORLH models being used in weak absorption scenarios of tokamaks with large aspect ratio.

Ⅰ. Introduction

Radio-frequency power in the lower hybrid range of frequencies (LHRF) has been used as an important tool in plasma current drive and plasma profile control in EAST long pulse discharges which are carried out in present experiments with plasma parameters: $B_0 \sim 2.0\ \mathrm{T}, R = 1.8\ \mathrm{m}, a = 0.45\ \mathrm{m},\ n_e \sim 1.0 - 3.0 \times 10^{19}\ \mathrm{m}^{-3},\ T_e \sim 1.0 - 2.0\ \mathrm{keV}$. The lower hybrid wave (LHW) system on EAST couples up to 2 MW of LHW power at 2.45 GHz into the EAST plasma through a 4×5 waveguide, and most of the power is coupled with refractive index parallel to the magnetic field ($n_{||}$) in the range of 1.5-3 **[Wan, 2009]** where $n_{//} = (k_{//}\ c\ /\ \omega)$ and $k_{//} = \mathbf{k} \bullet \mathbf{B}/\ |\mathbf{B}|$ is the wave number parallel to the applied magnetic field**.** Prior studies **[Bonoli, 1984]** indicate that the LHW is able to be absorbed efficiently by electrons through quasilinear Landau damping when the parallel phase velocity is low enough to satisfy $v_{||}/v_{Te} \approx 3$, where $v_{Te} = (2T_e/m_e)^{1/2}$. However, since the electron temperature in EAST is relatively low ($< 2\ \mathrm{keV}$), there is a large spectral gap between the launched $n_{||}$ and the $n_{||}$ at which the wave is able to damp efficiently.

Ray tracing – Fokker Planck models have been applied successfully to interpret LHCD experiments in a number of devices with moderate aspect ratio ~3, including Alcator C-Mod[**Schmidt, 2011][Wallace, 2010]**, FTU**[Barbato, 2011]** the JET tokamak **[Baranov, 1996]**, JT60-U**[Naito, 2002]**, and the Tore Supra tokamak **[Peysson, 2000][Decker, 2011]**. However, unlike these devices, EAST has a larger aspect ratio of ~4 ($R = 1.8\ \mathrm{m},\ r = 0.45\ \mathrm{m}$), which raises the question of how large the variation (upshift) will be in the parallel wavenumber due to the toroidal effect. In other words, the LHW is in a weak absorption regime and may undergo more passes before

damping completely in EAST than it does in other devices, which poses a challenge for the simulation of LHCD in EAST using ray-tracing models. Indeed past simulations of LH wave behavior in EAST **[Ding, 2011]** using the C3PO ray tracing code **[Peysson, 2012]** have shown that increases in the parallel wave number due to toroidally induced variations in the poloidal mode number (m) are sufficient to reduce the parallel phase speed to the point where quasilinear electron Landau damping is possible, i.e., $v_{\parallel}/v_{Te} \approx 3$. As expected, those simulations exhibited multiple passes of ray trajectories between the plasma core and the edge (cut-off). One of the goals of the present work is therefore to revisit these simulations using a ray tracing code that employs a scrape off layer (SOL) model **[Wallace, 2010]** in order to assess the effect of collisional damping of the LH waves which becomes important in the weak absorption regime where the LH wave undergoes multiple reflections in the SOL.

It is important to note that extensive theoretical and simulation research has been conducted to investigate alternate mechanisms for closing the spectral gap in LH current drive experiments, including scattering of LH waves from density fluctuations **[Bonoli, 1981], [Andrews, 1983], [Peysson, 2011], [Bertelli, 2013]**, **[Decker, 2014]** parametric decay processes**[Cesario, 2004][Cesario, 2010]**, full-wave propagation effects**[Wright, 2009][Shiraiwa, 2011][Meneghini, 2012],** diffraction effects and beam tracing**[Pereverzev, 1992]**, and magnetic ripple**[Bizarro, 1995]**, **[Peysson, 1996]**, and **[Bizarro, 1999]** . Indeed these effects may be present in the EAST experiments, however it was the primary goal of the present work to assess only the toroidal effect on wave propagation using the ray-tracing analysis. In fact modifications to the C3PO ray tracing code [**Peysson, 2011**] to take into account perturbations of the density due to turbulent fluctuations were found to reproduce hard x-ray measurements in the Tore Supra device when combined with the LUKE 3-D Fokker Planck code **[Decker, 2004, 2014].** A similar result was reported by Bertelli and co-workers **[Bertelli, 2013]** where they found that significant increases in the parallel

wave number could be induced by scattering of LH waves from density fluctuations in Alcator C-Mod plasmas. However the resulting power deposition profiles were qualitatively similar to what was found when only toroidal effects on the parallel wavenumber were considered, in large part due to the stochastic nature of the wavenumber variation which was studied previously by Kupfer **[Kupfer, 1993]**, Bizarro and Moreau **[Bizarro and Moreau, 1993] [Bizarro, 1993]**. The development of full-wave electromagnetic field solvers in the LHRF regime has helped to resolve some of the uncertainties related to proper treatment of weak absorption regimes, since reflection of the wave from caustic surfaces in the core and cut-offs in the edge plasma are now treated properly within the full-wave framework. Results from full-wave field simulations reported by Wright and Shiraiwa **[Wright, 2009][Shiraiwa, 2011]** showed that power absorption profiles from ray tracing and full-wave calculations were qualitatively similar, despite breakdown of the geometrical optics approximation at cut-offs and caustic surfaces. Simulations performed by Shiraiwa and Meneghini did find broader absorption profiles caused by large variations in the parallel wave number near the plasma edge, just inside the closed flux surface **[Shiraiwa, 2011] [Meneghini, 2012]**. Considering that it would be interesting to see if the full wave effects could play a significant role in bridging the large spectral gap in weak absorption scenarios of tokamaks with large aspect ratio, our second goal is to introduce the full wave code TORLH to the simulation of LH physics in the EAST and compare it with the ray-tracing.

In the research reported in this paper we have used the coupled GENRAY-CQL3D code, which is an advanced ray-tracing and Fokker-Planck analysis tool. The ray-tracing code GENRAY**[Smirnov, 1995]** solves the ray equations of the geometrical optics by integrating Eqs. (1a) and Eqs. (1b) in the Cartesian coordinate system,

$$\mathrm{dx/dt} = -(\partial\varepsilon\ /\ \partial\mathrm{k})/(\partial\varepsilon\ /\ \partial\omega)\ , \tag{1a}$$

$$\mathrm{dk/dt} = \ \ (\partial\varepsilon\ /\ \partial\mathrm{x})/(\partial\varepsilon\ /\ \partial\omega)\ , \tag{1b}$$

where $\mathrm{x} = (\mathrm{X}, \mathrm{Y}, \mathrm{Z})$ is the ray position, $\mathrm{k} = (\mathrm{k_X}, \mathrm{k_Y}, \mathrm{k_Z})$ is the wavenumber, and for the interest of the simulation of LHW, $\varepsilon(\mathrm{x}, \mathrm{k}, \omega)$ is the local dispersion relation

which is valid in the LHRF**[Bonoli, 1986]**. The wave electric field is calculated by GENRAY along the ray trajectory, and is then used to reconstruct the quasilinear diffusion coefficient (D_{RF}) for the coupling to the CQL3D Fokker-Planck code**[Harvey, 1992] [Kerbel, 1985]**. The CQL3D code is used to calculate the electron distribution functions by solving the momentum-space bounce-averaged Fokker-Planck equation in axisymmetric toroidal geometry resulting from a balance between RF quasilinear diffusion, collisions, dc electric field, and radial transport. The electron model used for the simulation of LHCD in EAST is written in the following 3-D form (two dimensions in momentum space ($p_\perp$, $p_{//}$) and one spatial dimension – (r)):

$$\frac{\partial}{\partial p_\parallel} D_{RF}(p_\parallel)\frac{\partial f_e}{\partial p_\parallel} + C(f_e, p_\parallel, p_\perp) + eE_\parallel \frac{\partial f_e}{\partial p_\parallel} + \frac{1}{r}\frac{\partial}{\partial r} r\chi_f \frac{\partial f_e}{\partial r} = \frac{\partial f_e}{\partial t} \quad (2)$$

where $f_e(p_\perp, p_\parallel)$ is the electron distribution function, $p_\perp$ and $p_\parallel$ are the component of momentum perpendicular and parallel to the magnetic field respectively, $E_\parallel$ is the DC electric field, $D_{RF}(p_\parallel)$ is the RF quasilinear diffusion operator which results from the presence of RF waves mentioned above, $C(f_e, p_\parallel, p_\perp)$ is the Coulomb collision term, and the last term on the left hand side of the equation is the radial transport diffusion term **[Rax, 1989][Fuchs, 1989]** with the fast electron diffusivity χ_f. The current density is then obtained from the $v_\parallel$ moment of the electron distribution function.

The TORLH code **[Wright, 2009]** that is also used in this paper is a full wave electromagnetic code, which solves a wave equation of the form:

$$\frac{c^2}{\omega^2}\nabla \times \nabla \times \vec{E} = S\vec{E}_\perp + iD(\vec{b} \times \vec{E}_\perp) + P\vec{E}_\zeta + \frac{4\pi i}{\omega}(\vec{J}_e^{(2)} + \vec{J}_{ANT}), \quad (3)$$

$$\frac{4\pi i}{\omega}\vec{J}_e^{(2)} = -\frac{c^2}{\omega^2}\nabla_\perp \times [\lambda_0(\nabla_\perp \times \vec{E}_\perp)] + i\frac{c^2}{\omega^2}\{\nabla_\perp \times [\xi_0(\vec{b}\cdot\nabla)\vec{E}_\parallel\vec{b} + \vec{b}(\vec{b}\cdot\nabla)[\xi_0\vec{b}\cdot (\nabla_\perp \times \vec{E}_\perp)]\}, \quad (4)$$

$$\lambda_0 = \frac{1}{2}\frac{\omega_{pe}^2}{\Omega_{ce}^2}\frac{v_{te}^2}{c^2}[-x_e Z(x_e)], \qquad \xi_0 = \frac{1}{2}\frac{\omega_{pe}^2}{\omega\Omega_{ce}}\frac{v_{te}^2}{c^2}[x_e^2 Z'(x_e)]$$

where S, D, and P, are the Stix components of the dielectric tensor, expanded in the LH range of frequencies ($\Omega_{ci} \ll \omega \ll \Omega_{ce}$). The primary damping mechanism for the LH wave is parallel electron Landau damping (ELD) which is given by the third term on the right hand side of Eq. (3). The second order electron finite Larmor radius FLR current is given by Eq. (4), where the first term on the right hand side represents transit time magnetic pumping (TTMP), and the second is the cross - term between ELD and TTMP. It can be easily shown that in the LHRF regime these terms are always small, being on the order of $(k_\perp \rho_e)^2$.

A semi - spectral ansatz [see Eq. (5)] is used in TORLH to represent the electric field in terms of poloidal (m) and toroidal (n) Fourier modes:

$$\vec{E}(\vec{x}) = \sum_{m,n} \vec{E}_{m,n}(\Psi) e^{im\theta + in\phi} \tag{5}$$

The radial dependence of the coefficients in Eq. (5) is expressed in terms of cubic Hermite interpolating polynomials. Full-wave simulations in the LHRF regime are especially challenging in EAST because of the large device size ($a \sim 0.45$ m) and the short perpendicular wavelengths. For example at $n_e \sim 1 \times 10^{19} m^{-3}$, $f_0 = 2.45$ GHz, and $n_{\parallel 0} = 2.1$, the cold plasma electrostatic dispersion relation yields $k_\perp \sim (f_{pe}/f_0) k_\parallel \sim 1.25\ mm^{-1}$. The spectral Ansatz in Eq. (5) implies that an upper limit on the poloidal mode number can be obtained by assuming $k_\perp \sim m/r$. Thus for $r \sim a = 0.45m$, one obtains $m \sim r \times k_\perp \sim 540$. Thus the poloidal mode expansion in Eq. (5) requires $-540 \le m \le +540$, or at least 1100 poloidal modes to resolve the incident LH wave. In the full wave simulations carried out for EAST we have taken 2047 poloidal modes ($-1023 \le m \le +1023$) and 480 radial zones in order to guarantee convergence of the full wave solver. The choice of the number of radial zones deserves some discussion. The value of $k_\perp \sim 1.25\ mm^{-1}$ quoted above is based on $n_\parallel = 2.1$. However $n_\parallel$ will increase to 5 and higher as the wave damps via electron Landau damping, which corresponds to $\lambda_\perp \sim 1mm$. Taking 480 radial

elements with a = 0.45m, implies only about one radial element per wavelength. However, TORLH is a semi-spectral code which uses finite elements (cubic Hermite interpolating polynomials) in the radial direction. There are therefore three sample points per radial zone or about 480 × 3 = 1440 radial points in a simulation. This then translates to about 3 radial points per perpendicular wavelength. Besides, a component of $k_\perp$ is in the flux surface and so is carried in part by the poloidal basis and so the resolution for perpendicular wavelength is generally higher than the number of radial elements would suggest. We have also carried out TORLH simulations with 980 radial zones or finite elements (2940 radial points or 6 radial points per wavelength) and not found the results to change significantly, thus giving some confidence that 480 radial zones is adequate. The mode resolution used in these simulations is equal to the highest mode resolution simulations carried out with TORLH to date.

This paper includes three main topics which are in section Ⅱ, Ⅲ, and IV respectively. First, we describe the GENRAY-CQL3D simulation for a low density LHCD experiment in EAST. The LHW physics in this case is investigated, and the model for the SOL **[Wallace, 2010]** that uses the magnetic geometry from an EFIT reconstruction **[Lao, 1985]** and exponentially decaying density and temperature profiles that are characterized by the experimentally measured decay lengths, thus making it possible to investigate the LHCD efficiency reduction caused by collisional damping which is proportional to $n_e/T_e^{3/2}$ is then introduced and included in the simulation to compare with the experiment. Next the radial transport effects of the fast LH electrons on the experimental level of LHCD are discussed. Then, the LHW physics in higher density discharges on EAST is also studied with the SOL model to give an interpretation to differences seen experimentally between the relatively weaker and stronger absorption discharges. Finally, in order to assess the relative importance of effects such as wave diffraction which are not included in the geometrical optics approach as well as to treat wave behavior properly at caustics

and cut-offs, we also show simulation results for LH power absorption in a low density case that were obtained using the TORLH electromagnetic field solver.

Ⅱ.Simulation of LHCD experiments in low density case of EAST

A. Experimental parameters for low density case of EAST

In the past a few years, LHCD played a key role in several significant experimental results on the EAST tokamak, such as obtaining H-mode using LHCD only and using the combined injection of LHCD and ICRH**[Wang, 2012],** and the observation of co-current toroidal rotation associated with LHCD**[Shi, 2011]**. In the latter discharge, 250 kA of plasma current was mainly driven by 800 kW of LHW power coupled to an EAST plasma with line average density of $\sim 0.8 \times 10^{19}\,\mathrm{m}^{-3}$ and electron temperature of ~1.5 keV with the loop voltage being driven to zero. Simple calculation indicates that in this low density case, LHW rays satisfied the accessibility condition **[Troyon, 1974; Brambilla, 1979]** at the plasma core [see Eq. (6)] and thus could penetrate to the plasma center.

$$n_{\parallel} > n_{\parallel,\mathrm{crit}} = \frac{\omega_{\mathrm{pe}}}{\Omega_{\mathrm{ce}}} + \sqrt{1 + (\frac{\omega_{\mathrm{pe}}}{\Omega_{\mathrm{ce}}})^2 - (\frac{\omega_{\mathrm{pi}}}{\omega})^2}\ , \tag{6}$$

where $\omega_{\mathrm{pe}} = (\frac{n_e e^2}{\varepsilon_0 m_e})^{1/2}$ is the electron plasma frequency, $\Omega_{\mathrm{ce}} = eB/m_e$ is the electron gyro-frequency and $\omega_{\mathrm{pi}} = (\frac{n_i Z_i^2 e^2}{\varepsilon_0 m_i})^{1/2}$ is the ion plasma frequency.

Despite the very low electron temperature and subsequent multiple passes of the LH rays, a significant level of current was driven by the LHW due to weak losses via collisional damping compared with the cases described in the next section. As a starting point in the analysis, this case was chosen to be simulated by GENRAY-CQL3D, to study the behavior of LHW in the low density EAST regime, and to compare the GENRAY-CQL3D prediction with experiment. The plasma parameters which are close to the ones in [Shi, 2011] and used in the simulations shown in the next section correspond to an EAST discharge 011037 at a time of 4.30 sec., toroidal magnetic

field B_t = 2.0 T, total plasma current I_p = 250 kA, deuterium plasma, $n_e(0) = 1.0 \times 10^{19}$ m^{-3}, $n_D(0) = 0.9 \times 10^{19}$ m^{-3}, $n_e(a) = 0.4 \times 10^{19}$ m^{-3}, $n_D(a) = 0.4 \times 10^{19}$ m^{-3}, $T_e(0)$ = 1.5 keV, $T_D(0)$ = 0.5 keV, $T_e(a)$ = 0.05 keV, $T_D(a)$ = 0.05 keV, and analytic profiles for density and temperature were taken to be of the form:

$$n_{e,i}\,(\rho) = [n_{e,i}(0) - n_{e,i}(a)][1 - \rho^2]^{0.5} + n_{e,i}(a), \qquad 7(a)$$

$$T_{e,i}\,(\rho) = \left[T_{e,i}(0) - T_{e,i}(a)\right][1 - \rho^2]^{1.0} + T_{e,i}(a). \qquad 7(b)$$

B. LHW physics investigation using ray-tracing in the low density case

The spectrum of the LHWs was calculated based on Brambilla's theory [Brambilla, 1976] using the parameters of the LHW system on EAST with zero phase difference between two adjacent subwaveguides. As can be seen in Fig.1, most of the LHW power was launched with parallel refractive index peaked at the value around 2.1. According to the discussion above, a large spectral gap exists between this value and the value that the Landau damping condition requires ($n_{//}$ ~ 6-7 at T_e ~ 1 keV). And based on the experimental information given in Part A, the GENRAY simulation using a single ray with $n_{\|} = -2.1$ launched at the midplane shows that the ray undergoes multiple passes before its power is completely damped as shown in Figs. 2(a) and 2(c). An artificial specular reflection from the LCFS for the ray was used in this simulation, and it's important to point out that the specular reflection based on the geometrical-optics law was not formally generalized to plasma-wave rays in a magnetically confined plasma until 2010**[Bizarro, 2010]**. The ray behavior seen in Figs. 2(a) – 2(c) is well-known (see the discussion below), where after a radial reflection from a position near the bottom (or top) of the tokamak (depending on the sign of the poloidal field) the poloidal mode number and $n_{//}$ of the ray increase rapidly as the wave propagates into the core. Note the direction of B_t is clock-wise and I_p is counter-clockwise if the EAST tokamak is viewed from the top. Thus to

drive a co-current with the LH launcher it is necessary to use a negative value of $n_{//}$ = -2.10.

The power deposition profile was also modeled using 100 rays (20 rays each launched from five different poloidal locations with a single lobe in the power spectrum around $n_{\parallel}(0) = -2.1$) which is moderate for keeping the balance between the wave damping and the nearby ray trajectories' divergence **[Bizarro and Moreau, 1993] [Bizarro, 1993]** in the GENRAY simulation for the same case (T_e=1.5 keV) shown in the Fig. 3(red curve). The peaks of power density are off-axis even though there is no accessibility condition limitation since the density is low. An examination of the LH ray trajectories from GENRAY indicates that the off-axis nature of the LHW power deposition is related to the following: First the phase velocity of the incident wave is too high to damp on tail electrons at $3V_{te}$ on the initial pass of the wave front into the plasma core. Consequently the rays undergo multiple radial reflections at the plasma edge. As can be seen in Fig. 2(a), the radial reflection points move around poloidally as the ray trajectory advances until there is a reflection near the bottom of the cross-section. After this reflection the poloidal component of **k** undergoes large increases **[Ignat, 1981] [Bonoli, 1982]** as the ray propagates into the plasma that result in concomitant increases in $k_{\parallel}$ through the poloidal field. We note that this phenomenology has been studied in the past and has been shown to be related to the poloidal inhomogeneity in the toroidal magnetic field **[Bonoli, 1982]**, whose magnitude depends on the inverse aspect ratio(a/R_0). An important finding of the present work is that the stochastic nature of the ray trajectories**[Kupfer, 1993]** that derives from these aspect ratio dependent variations in the poloidal component of **k** and $k_{\parallel}$, are found to occur in the EAST device where the aspect ratio $A = R_0/a = 1.8/0.45 = 4.0$ is significantly higher than in other devices such as Alcator C-Mod where $A = 0.66/0.22 = 3.0$. Thus, in the low temperature (~1.5 keV) case where the spectral gap is large, the wave damping on electrons relies very much on the upshift of the parallel wavenumber due to toroidal effect or other effects not

included in ray-tracing such as diffraction**[Wright, 2009][Meneghini, 2009]** which is beyond the scope of this section. For comparison, we rerun the scenarios with the electron temperature increased to 2.5 keV and 3.5keV, and more power tends to damp towards the plasma center when the temperature is higher, as shown in Fig. 3 with the green curve (2.5keV) and blue curve (3.5keV) respectively. Presumably in those cases the higher core electron temperature allows more seed electrons to be created in the plasma center at $v_{\parallel} \sim 3V_{te}$ on the initial passes of the LH wave front into the core. In performing the ray simulations at the higher temperatures in Fig. 3 (2.5 keV and 3.5 keV curves) the magnetic equilibrium was not re-calculated at the higher electron temperatures. The intent in varying only the electron temperature in Fig. 3 was to isolate (in a parametric sense) the effect of the temperature variation in the weak damping limit. Prior studies of LHCD have achieved MHD equilibria consistent with the LH current drive source by iterating between an MHD solver and the current drive calculation **[Bonoli, 1990] [Devoto, 1992]**. These studies indicate that the LH current density profile changes primarily due to changes in the poloidal magnetic field as the MHD equilibrium is re-solved. Of course the MHD equilibrium changes due to variations in the pressure profile (kinetic profiles) and due to changes in the total parallel current density (which includes the LH current density source term). Thus strictly speaking changes in the kinetic profiles could affect the ray behavior. It is interesting to note that the LH power deposition profile of the case with $\mathrm{T_e} = 1.5\ \mathrm{keV}$ in Fig. 3 is qualitatively similar to the simulated profiles shown in the work by Shi [Shi, 2011] in terms of off axis characteristic.

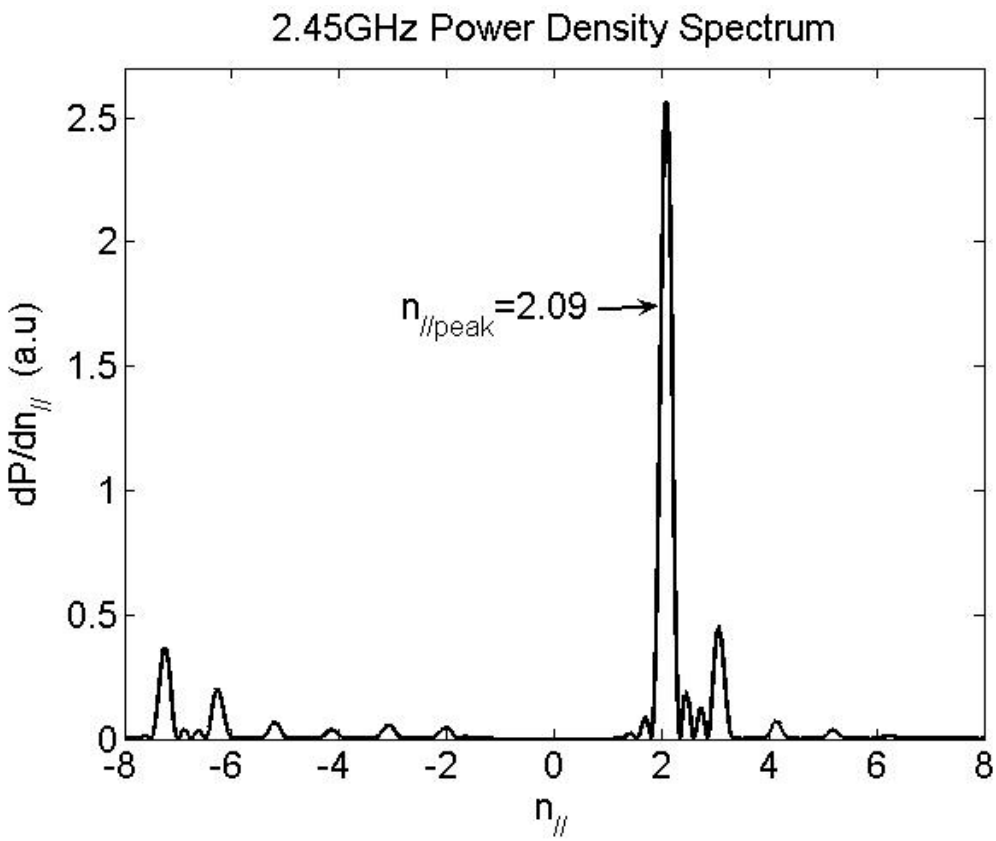

Figure 1 The spectrum of the LHW calculated based on Brambilla's theory [Brambilla, 1976] using the parameters of the LHW system on EAST with zero phase difference between two adjacent subwaveguides.

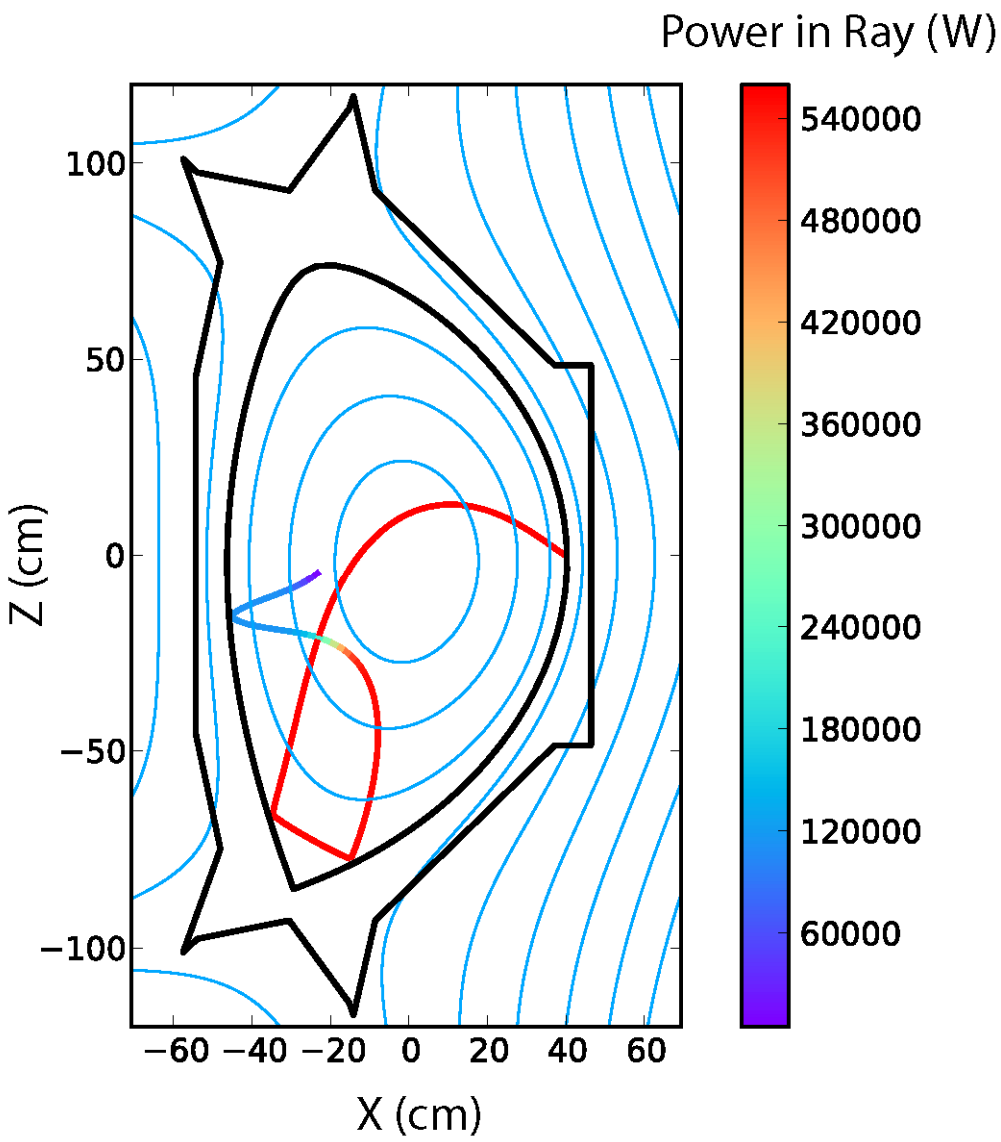
Power in Ray (W)
540000
480000
420000
360000
300000
240000
180000
120000
60000
100
50
0
−50
−100
Z (cm)
−60
−40
−20
0
20
40
60
X (cm)

Figure 2(a)

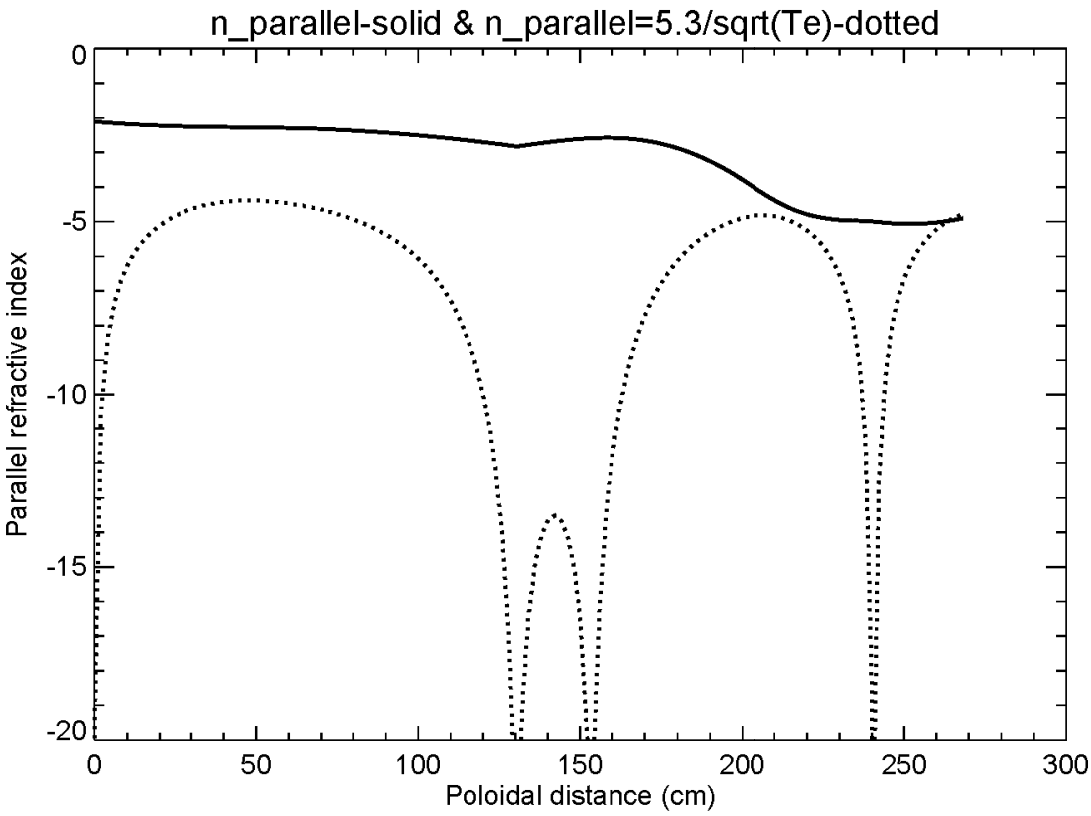

Figure 2(b)

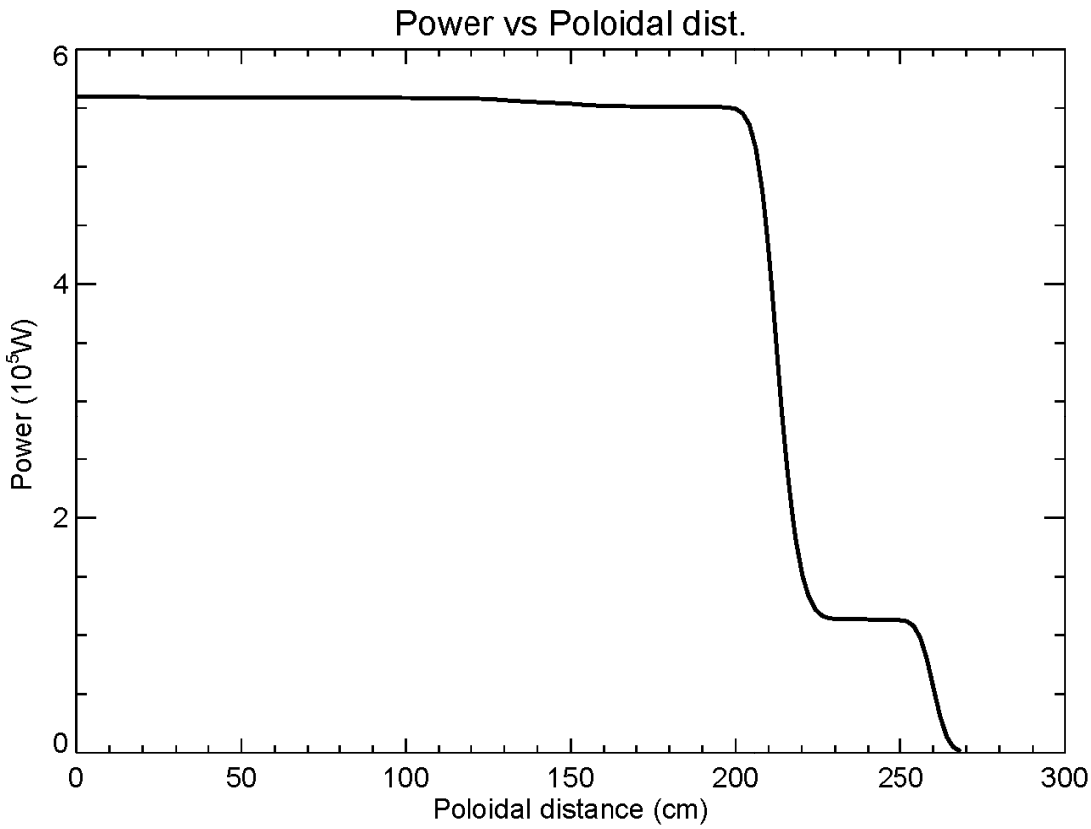

Figure 2(c)

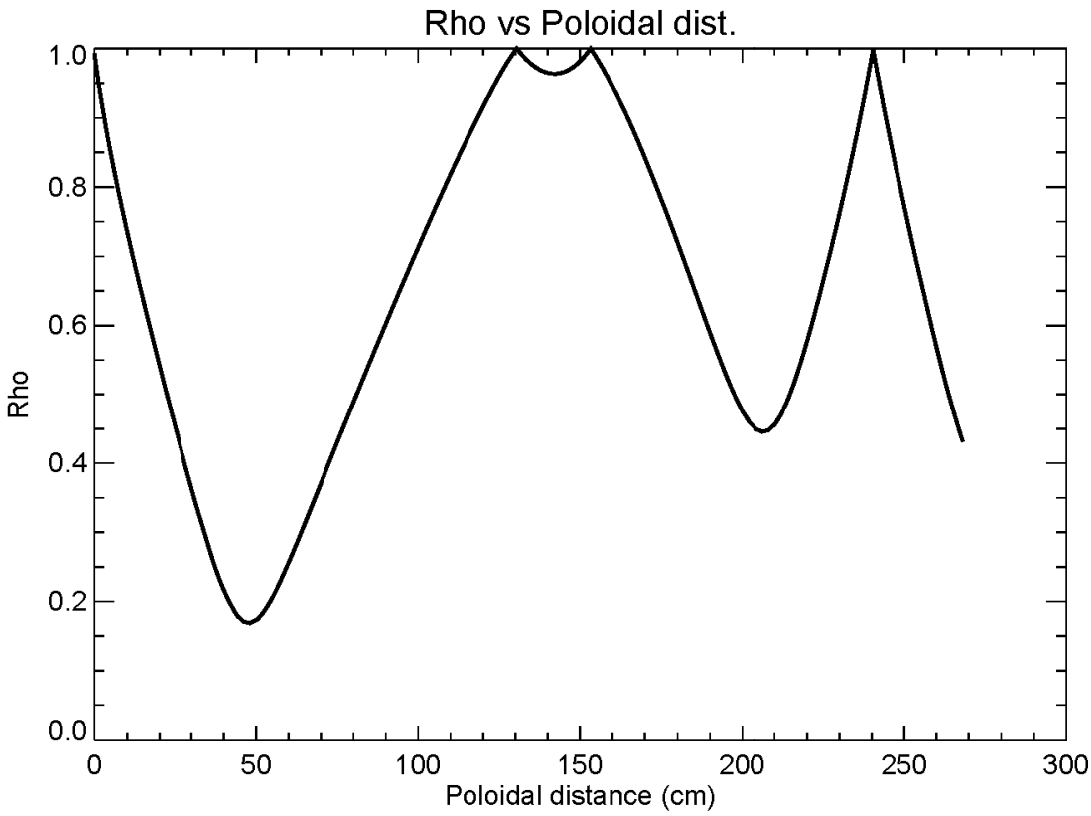

Figure 2(d)

Figure 2 GENRAY ray-tracing analysis of the LHW in the EAST scenario with line average density of $\sim 0.8 \times 10^{19}\ \mathrm{m}^{-3}$, and electron temperature of ~1.5 keV. A single ray was launched from the mid-plane position in the cross-section with $\mathrm{n}_{\parallel 0} = -2.1$, and the launched power was 0.56 MW which was 70% of the total experimental value of ~0.8 MW based on the spectrum shown in Fig.1 approximately. (a) The trajectory of the single ray with color coded power damping along its path (b) The solid line shows the variations of the $\mathrm{n}_{\parallel}$ and the dotted line shows $\mathrm{n}_{\parallel}$ required by the linear Landau damping absorption condition $(\omega/(\mathrm{k}_{\parallel}\mathrm{v}_{\mathrm{te}}) = 3$, where $\mathrm{v}_{\mathrm{te}} = \sqrt{2\,\mathrm{T}_{\mathrm{e}}/\mathrm{m}_{\mathrm{e}}}$, and $\mathrm{n}_{\parallel} = \mathrm{k}_{\parallel}\mathrm{c}/\omega$) along the ray path. The x label 'Poloidal distance' refers to the distance in cm (centimeter) traveled by the LH ray projected into the poloidal plane. (c) The power in ray along the ray path. (d) The r/a versus poloidal distance traveled by the ray.

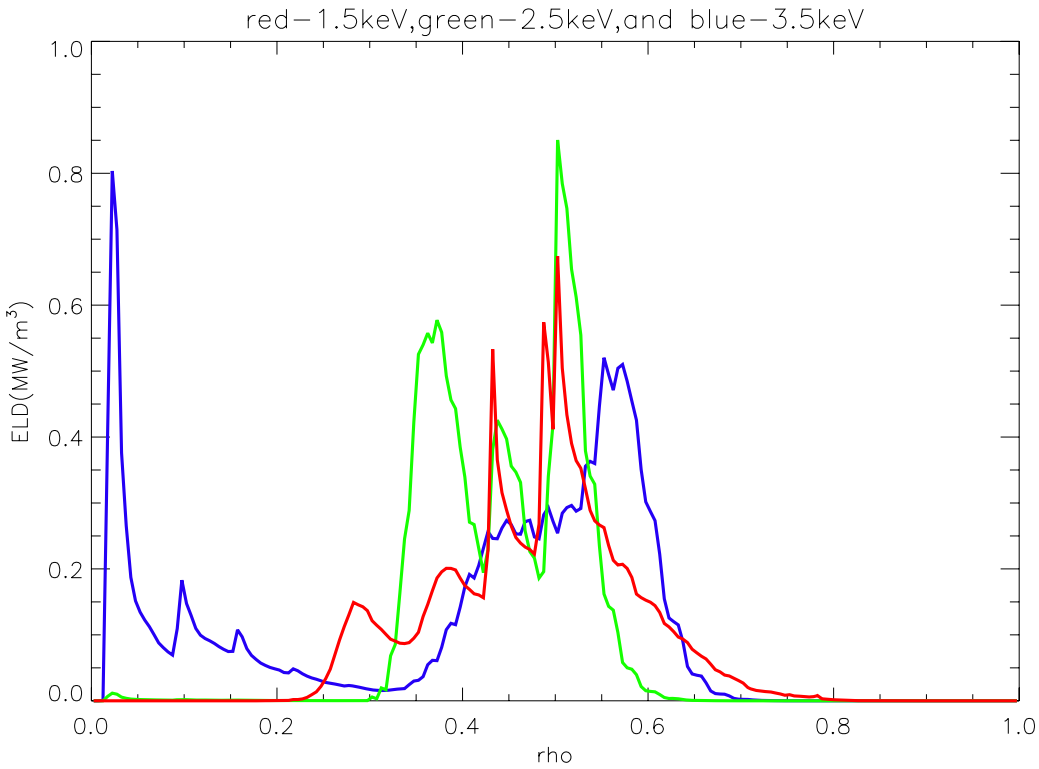

Figure 3 Radial power density profiles for 1.5 keV (red curve), 2.5keV (green curve) and 3.5keV (blue curve) cases.

The integrated LH power is 1MW in each case.

C. Collisional damping of LHW

The LHW can be absorbed in the plasma either by electron Landau damping or by collisions. Although the ray trajectory shown in Fig. 2 did not undergo many passes before its power was completely damped via electron Landau damping, this is not found to be the case for many of the rays, which undergo more radial reflections at the edge before damping by electron Landau interaction. It is therefore of great interest to introduce a SOL model as is done in the next section in order to calculate how much of the LH power might be absorbed by electron-ion and electron-electron collisions, especially when the ray propagates out to the SOL where it reflects from the cut-off layer. The calculation of RF damping using linear codes is usually done in the weak damping limit by adding an imaginary part to the dispersion relation. In the GENRAY simulation, to calculate the collisional damping, the electron mass m_e is

replaced by $m_e(1+\frac{i\nu_{ei}}{\omega})$ in the cold plasma dispersion relation, where ν_{ei} is the effective electron-ion momentum collision frequency which is proportional to $n_e/T_e^{3/2}$ **[Bonoli, 1986]**. Typically in the tokamak plasma core the electron-ion collision frequency is much less than the LH wave frequency. However, in the area near the LCFS or in the scrape off layer where the temperature is extremely low and the electron Landau damping can be neglected, the collisional damping may dominate. The LH power absorbed by collisions is not able to drive current directly. Thus for the weak absorption case where significant power is lost via collisions during multiple passes of rays between the low density cut-off layer and the high density limit associated with the accessibility condition, there is the potential for the current drive efficiency to be reduced significantly.

D. SOL model in the GENRAY simulation

A new capability of the GENRAY code makes it possible to employ the actual SOL model with magnetic field, density, temperature, and geometry into the simulation. The magnetic field geometry in the SOL is imported directly from the equilibrium reconstruction using the EFIT code **[Lao, 1985]**, with the geometry of the vacuum vessel and limiter also set up for the GENRAY simulation. Both the density and the temperature outside of the LCFS are assumed to fall off exponentially in the radial direction, which can be described by the following formulas respectively:

$$n_\rho = n_{LCFS} \times e^{(-(\rho-1)/\sigma_n)} \tag{8a}$$

$$T_\rho = T_{LCFS} \times e^{(-(\rho-1)/\sigma_T)} \tag{8b}$$

where $n_{LCFS} = n_{e,i}(a)$ and $T_{LCFS} = T_{e,i}(a)$ are the electron and ion densities and temperatures at the LCFS respectively, and σ_n and σ_T are the normalized (to plasma radius) exponential density and temperature decay lengths outside of the LCFS starting at $\rho = 1$ respectively. In setting up the GENRAY simulations, measurements of the “near” SOL plasma parameters reported in [Shi, 2011] have

been used where $n_{LCFS} = 0.50 \times 10^{19}$ m^{-3}, $T_{LCFS} = 25$ eV, $\sigma_n = 0.05$, and $\sigma_T = 0.05$.

Note that the SOL model is only included in the GENRAY code but not in the CQL3D, so the information from rays absorbed in the SOL is not used directly in the calculation of the quasilinear diffusion coefficient for CQL3D. However, with the SOL model in the simulation, the current drive inside of the LCFS calculated by CQL3D should be more accurate because the actual power lost via collisions does not drive current and is therefore excluded in current drive calculation inside of the LCFS. Futhermore, those rays with higher parallel wave numbers **[Bonoli, 1986]** are more strongly absorbed in the SOL due to collision, resulting in a modification of the spectral shape of the quasilinear diffusion coefficient which can then change the electron distribution function evolved in the Fokker-Planck calculation.

E. GENRAY/CQL3D simulation for calculation of LHCD including the scrape off layer

For the simulations presented in this section the SOL model was included in GENRAY allowing the rays to reflect from the low density cut off in the SOL. Using the experimental information given in Part A and 200 rays (20 rays with $n_{\|}$ around 2.1, 10 rays with $n_{\|}$ around 3.1, and 10 rays with $n_{\|}$ around -7.35 respectively launched from each of 5 poloidal locations) for the power spectrum shown in Fig.1, the GENRAY/CQL3D simulation was set up for the EAST plasma described earlier (discharge 011037 at a time corresponding to 4.30 sec with $B_0 \sim 2.0\ \mathrm{T}, R = 1.8\ \mathrm{m}, a = 0.45\ \mathrm{m}, \mathrm{and}\ I_p \sim 250\mathrm{kA}$). Since the plasma density was very low, the bootstrap current was not taken into account in the CQL3D analysis.

The collisional damping calculated by the GENRAY code in this case was 18.5% and the Landau damping was 81.5%, which confirms our thought that the collisional damping could not be neglected although the plasma density is not very high in this case [$n_e(0) = 1 \times 10^{19}$ m^{-3}]. Coupling the results from GENRAY to CQL3D, the

calculated LHCD in the case without radial transport turned on is 451 kA which is significantly higher than the value inferred from experiment (250 kA). Spatial diffusion of electrons, especially the fast electron tail in low density radiofrequency current drive cases, may play an important role. Fast electrons generated by LH waves in EAST are in the 100 keV range and higher. Thus they require $\tau_s \sim 0.03\text{sec}$ to thermalize at an electron density of $n_e \sim 1.0 \times 10^{19}\ \text{m}^{-3}$. The bulk energy confinement time in EAST discharges maintained by LH current drive has been found **[Gao, 2010]** to follow the ITER-89P scaling law, which for the discharge under study in this section is $\tau_e \sim 0.06 - 0.07\text{sec}$.. An estimate of the fast electron confinement time can be obtained from the measurements of runaway electrons in PLT **[Mynick, 1981]** where it was found that nonthermal electrons are better confined than the bulk electrons with a confinement enhancement for the fast electrons roughly following $\tau_F / \tau_E \approx \gamma^{\alpha}$, where γ is the relativistic factor, with $\alpha \approx$ 3-4. It is argued in **[Mynick, 1980, 1981**] that the runaway confinement is enhanced at higher electron energy due to phase averaging over magnetic perturbations when the runaway electron drift surfaces are displaced from the magnetic surfaces. This is in contrast to earlier work **[Rechester, 1978]** which only considered transport due to magnetic stochasticity with electrons running along a single perturbed magnetic field line. For LHRF-generated electrons at energies of 100 keV we have $\gamma^3 \approx 1.71$ and $\tau_F \sim 0.12$ sec. Thus it is reasonable to expect that a fast electron can diffuse spatially some distance as it slows down in velocity space since $\tau_s/\tau_F \sim 0.25$. Since the energies of the fast electrons in these experiments are only mildly relativistic we take an explicit form for the fast electron diffusivity (χ_F) in the Fokker Planck simulations that is independent of velocity and radius. The LH current driven in scenarios with different values of the fast electron diffusivity [$\chi_F(0)$] are calculated respectively, as shown in the following Figs. 4.

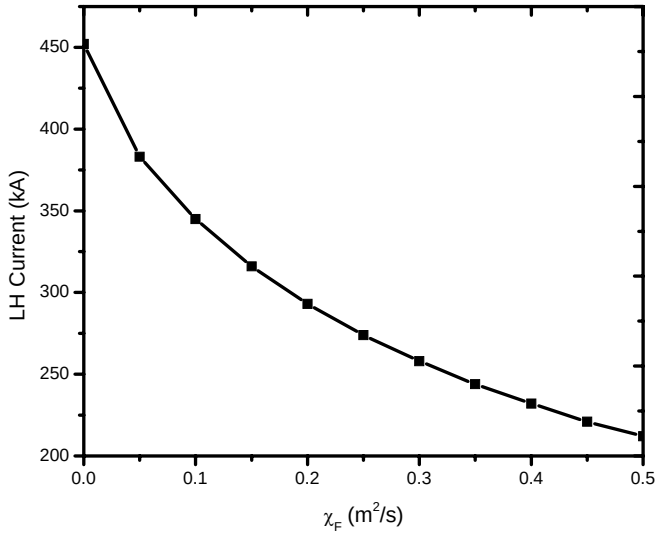

Figure 4(a)

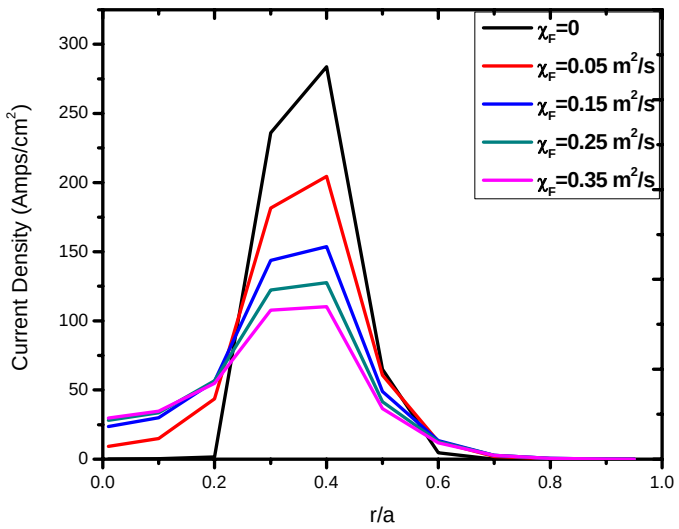

Figure 4(b)

Figure 4 (a) Integrated LH current (kA) and (b) Radial current density profiles with various values of radial transport diffusion coefficient χ_F (m^2/s). The integrated LH power was around 650 kW (800 kW * 81.5%) from Landau damping as stated above.

According to the results in Fig. 4, the current drive decreases as the radial transport increases, and when the diffusion coefficient is $0.3 - 0.35\ \mathrm{m}^2/\mathrm{s}$, the simulated

LHCD is closest to the value from experiment. This result is much lower than the value of ~ $1\ \mathrm{m}^2/\mathrm{s}$ which was found on PBX-M **[Jones, 1993]** but close to the value between $0.1 - 0.3\ \mathrm{m}^2/\mathrm{s}$ which was found on Tore Supra also in the low density regime**[Peysson, 1993]**. It is interesting to note that the magnitude of χ_F found to be consistent with the experimental level of current in EAST is also consistent with the simple scaling arguments for τ_F discussed above; where in cylindrical geometry χ_F can be approximated as $\chi_F \approx a^2/6\tau_F \sim 0.3\ \mathrm{m}^2/\mathrm{s}$, assuming a = 0.45m and τ_F ~ 0.12 sec. Note the factor of 6 in the expression for χ_F comes from solution of the fast electron current diffusion equation in cylindrical geometry where the solution for J_{RF} is the Bessel function $J_0(z)$**[Rax, 1989]**. Imposing a boundary condition of vanishing fast electron current at the boundary (r=a) yields $z = a/(\chi_F\tau_F)^{0.5} \sim 2.4$, corresponding to the first zero of the Bessel function**[Fuchs, 1989]**. The GENRAY / CQL3D simulations shown in Fig. 4 were quite challenging in order to maintain good convergence between power damped via ELD in the ray tracing and the power damped via quasilinear ELD in the Fokker Planck code, primarily because of the presence of the radial diffusion operator. The simulations were typically run out to 0.05 sec. (a few slowing down times) in order to achieve a fully relaxed distribution function. Furthermore it was necessary to take small times steps (~ 0.5×10^{-4} sec.) in order to maintain convergence between the ray tracing and Fokker Planck codes, with the power deposition and updated RF diffusion coefficient being recalculated along the ray trajectory paths every 0.5×10^{-4} sec., as the codes were iterated. The injected LH power used in the simulations was 800 kW and typically the powers from ray tracing and Fokker Planck agreed to within 5% in steady state. By comparing the current density profiles obtained from the cases with and without radial diffusion, one concludes that a modest amount of radial transport can smooth the structures of the profile significantly and the fast LH current is then redistributed and broadened. It is also important to mention that ray trajectories launched from different poloidal positions undergo different variations in the parallel wavenumber which also tends to spread the deposition location in both spectral and configuration space. Finally, by an appropriate value of the diffusion coefficient combined with

accounting for collisional losses in the SOL, the experimental level of LHCD is obtained in the GENRAY-CQL3D simulation.

Ⅲ. Simulation of LHCD experiments in higher density regime of EAST

A. Ray accessibility studies for higher density case of EAST

According to LHW physics theory, the LHW is able to penetrate into the plasma only if it satisfies the accessibility condition which is given by equation (6) **[Troyon, 1974; Brambilla, 1979]**. The GENRAY analysis indicates that, for an EAST equilibrium corresponding to discharge 039430 with $\mathrm{B_0 = 1.8T}$, $\mathrm{I_p = 386kA, and\ T_e(0) = 1.5\ keV}$, when the plasma density is increased to $4.0 \times 10^{19}\ \mathrm{m^{-3}}$, the ray is not able to propagate into the plasma with its initial value of $\mathrm{n_{||}}\sim 2.1$ until toroidal effects give rise to sufficient up-shift of $\mathrm{n_{||}}$ via multiple reflections from the plasma edge, as shown in Figures 5. A scrape off layer model was not used for the ray tracing analysis shown in Fig.5. Instead, when rays reached the last closed flux surface (LCFS) a specular reflection was introduced**[Bizarro, 2010]**. It is important to point out the ray tracing description is suspect after multiple reflections between cut-offs at the edge and the plasma edge as shown in Fig. 5, since the geometrical optics approximation breaks down in those regions. However in a qualitative sense, the ray behavior in Fig. 5 clearly makes the point that penetration of the LH wave fields is severely limited by wave accessibility at the upper end of the density regime in which LHCD experiments have been conducted on EAST [Ding, 2013].

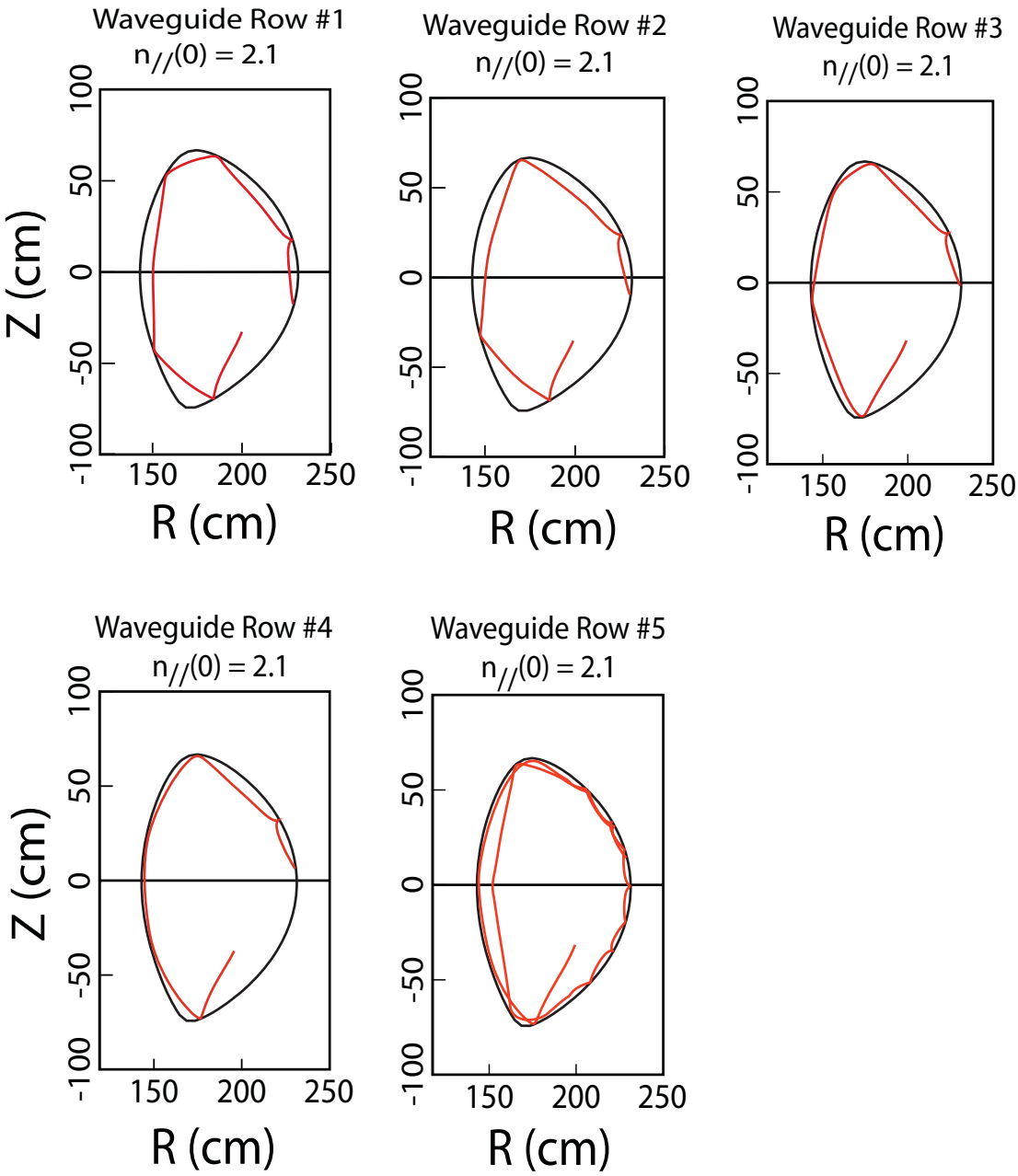

Figures 5: Ray trajectories computed by the GENRAY ray tracing code for poloidal locations corresponding respectively to waveguide rows #1, #2, #3, #4, and #5 of the EAST LH launcher. The black curve represents the LCFS and the red curve represents the ray trajectories. The parameters used here correspond to the EAST discharge 039430 at time of 3.00 sec. with B_0 = 1.8 T, I_p = 386 kA, $T_e(0)$ = 1.5 keV, $n_e(0) = 4 \times 10^{19}$ m^{-3}.

A significant fraction of the power for rays typical of those shown in Figures 5 might be deposited through collisional damping in the area near the Last Closed Flux Surface before the rays undergo enough up-shift of $n_{||}$ to penetrate deeper. Although a SOL model was not included in the analysis shown in Fig. 5, it would not

be expected that the inclusion of the SOL model would change the conclusions of this section with respect to wave accessibility at this high density. The SOL model will be included in the following GENRAY simulations which are going to be compared with the experiments, as it was done in the Section Ⅱ E.

B. Experimental results.

Lower hybrid waves were coupled into the discharges 039430 and 039440 in the 2012 campaign of EAST. Figures 6(a) and (b) show the time evolution of plasma current, plasma density, loop voltage, LHW power, and ICRF power in those two discharges. We are only interested in the time during these discharges prior to the injection of ICRF power during the flat-top density phase from 2 sec. to 4 sec., and we have taken a time at the midpoint for our analysis (3.00 sec.). After the ICRF power is turned on at 4.00 sec., the density starts to increase rapidly to $6 - 8 \times 10^{19}$ m^{-3}. At this point all wave accessibility is lost to the plasma and the wave power likely undergoes parasitic losses in the SOL due to collisional damping of the LH waves (as shown below) and / or parametric decay of the pump wave into ion sound quasimodes. In fact this latter effect has been observed in EAST discharges as the density increases beyond line averaged values of 3.5×10^{19} m^{-3} **[Ding, 2013]**. Based on experimental observations, the electron temperature in both discharges before turn on of the ICRF heating (at 3.00 sec.) is about 1.5 keV, which again results in a large gap between the launched $n_{\|}$ with a main peak value of 2.1 and the slower wave velocity (higher $n_{\|}$) at which effective Landau damping occurs. Before ICRF power is coupled, the plasma electron density as well as the total plasma current in steady state in the two discharges is almost the same (~386kA) consisting of both LHCD and current from Ohmic heating with loop voltage around 0.5-0.6 V. However the LHW power injected into the discharge 039440 (~1.65MW) is significantly higher than that into the discharge 039430 (~1.2MW). Thus these plasmas present a puzzling observation whose interpretation in terms of the ray tracing / Fokker Planck

framework is indeed a challenge.

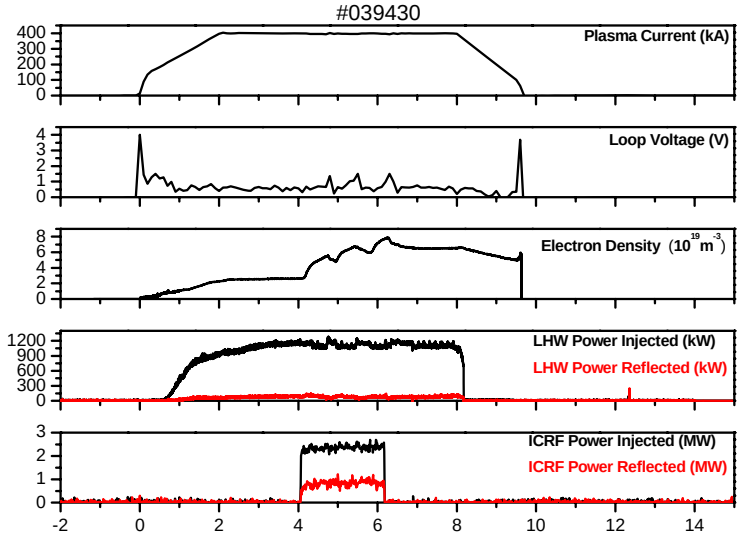

Fig. 6(a)

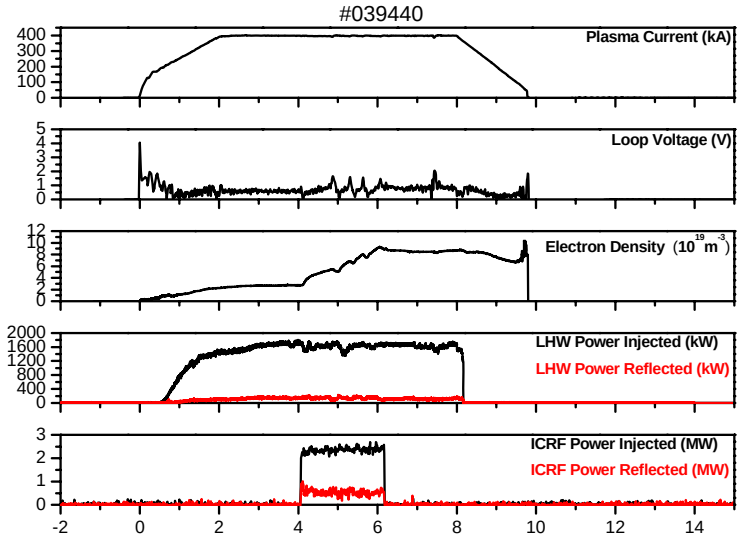

Fig. 6(b)

Fig. 6 Experimental traces from EAST showing the time evolution of plasma current (kA), plasma density ($10^{19}\mathrm{m}^{-3}$), loop voltage (V), LHW power (kW), and ICRF power (MW) in (a) the discharge 039430 and (b) the discharge 039440. In the stage before the ICRF is injected, the total steady state current in the discharge 039430 is driven by the Ohmic with loop voltage ~0.5 V and the LHW (~1.2 MW injected and ~0.1 MW reflected), and in

the discharge 039440 it is driven by the Ohmic with loop voltage ~0.5 V and the LHW (~1.65 MW injected and ~0.15 MW reflected).

C. Simulation of LHCD in the two discharges of EAST

The GENRAY-CQL3D simulation of LHCD was set up for the two EAST discharges 039430 and 039440 at 3.00 sec., with the SOL model included in the GENRAY code. The experimental observations of the kinetic profiles were used along with equilibria which are obtained from the experimental discharges and reconstructed using the EFIT code. The plasma parameters were set as follows: Inside of the LCFS, we use analytical parabolic radial profiles for both density and temperature, with central plasma density equal to $3.0 \times 10^{19}\ \mathrm{m}^{-3}$, an edge density equal to $0.8 \times 10^{19}\ \mathrm{m}^{-3}$, central electron temperature equal to 1.5 keV, and an edge electron temperature equal to 0.03 keV [Eqs. (7)]; Outside of the LCFS, we use the exponential fall off formulas given above [Eqs. (8)] with the normalized (to minor radius) decay length equal to 0.05 for both temperature and density for all poloidal angles.

GENRAY analysis of single ray trajectory indicates that the LHW was in the weak absorption regime for both discharges, which is shown in Figure 7:

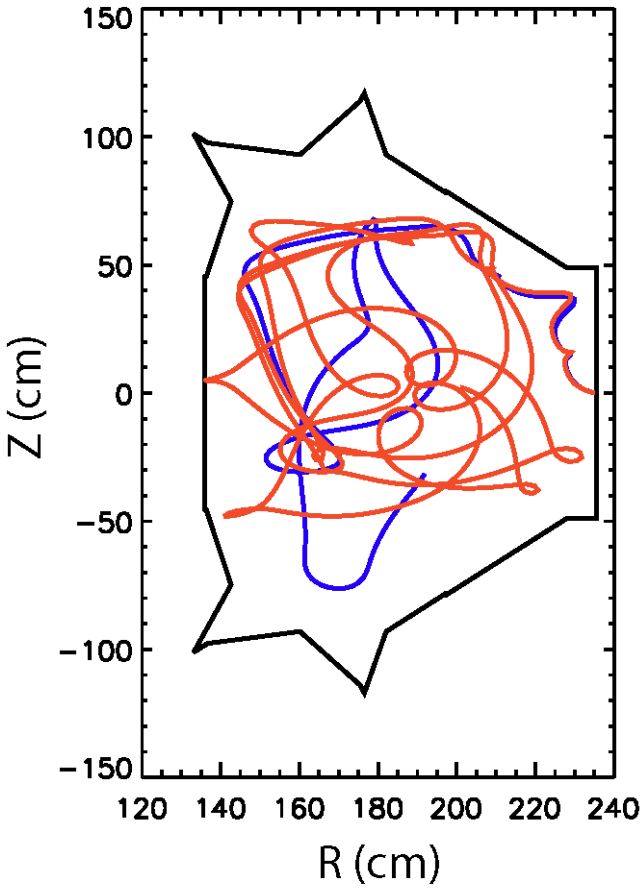

Figure 7(a)

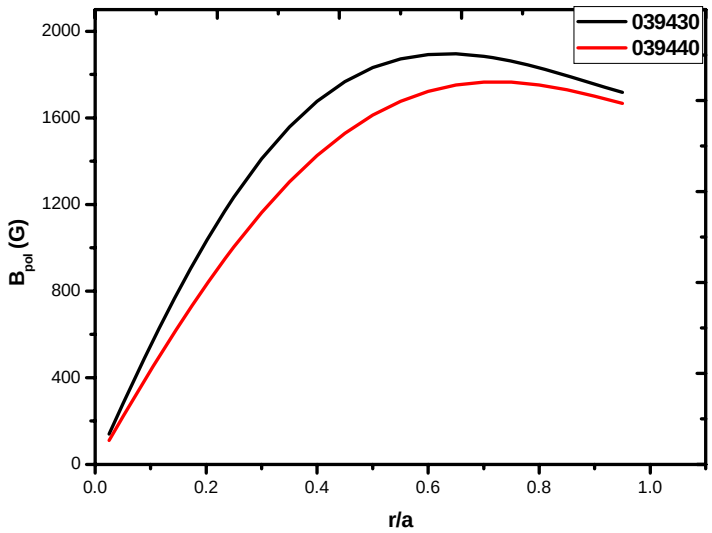

Figure 7(b)

Fig. 7 (a)With the initial value of parallel index of ~2.1, a single ray trajectory was simulated using the GENRAY respectively for the discharge 039430 (blue curve) and the discharge 039440 (red curve). The rays are reflected either by the low density cut-off layer or by the wall. The position of the launcher is given by (R,Z)

coordinates which are fixed according to the experimental set-up, so the distance between the launcher and the LCFS was calculated automatically in the simulation for different discharges with different outer gaps. Note that the LH rays are launched in different discharges, so the LCFSs are not drawn to avoid being a mess. (b) The radial profiles of the poloidal magnetic field of the discharges 039430 and 039440. Although the currents in the two discharges were the same, due to the different small radii and the different elongations and triangularities, the poloidal magnetic field in the discharge 039430 was about 10% higher than that in the discharge 039440.

An important difference between the two cases is that the ray undergoes fewer passes in the discharge 039430. After examination, this is primarily because the poloidal magnetic field (shown in Fig.7(b)) in the discharge 039430 is 10% higher than that in the discharge 039440 which gives rise to a larger up-shift of $n_{\|}$ due to toroidal effects in the discharge 039430. It's important to note however that the single ray is not the case for the following GENRAY-CQL3D simulation where 200 rays are used as was done in the Section Ⅱ.

To compare the power deposition distribution in the two discharges with the same level of LH power, we assumed the launched power was 1.2 MW in each discharge with 0.84 MW in the main peak at $n_{\|}\sim 2.1$, 0.18 MW in the secondary peak at $n_{\|}\sim 3.1$ and 0.18 MW in the reverse LH lobe at $n_{\|}\sim 7.35$ for both discharges. Also for comparison, the case without the SOL in the two discharges was simulated. The SOL was eliminated completely by turning on the artificial reflection from the LCFS, and the LH grills are assumed to be located right at the LCFS. Table (1) shows the partition of LH power between electron Landau damping and collisions in the above cases.

Table 1 Partition of LH power between electron Landau damping and collisions in the cases with the SOL and without the SOL for the two discharges

case	ELD (%)	Collision (%)
LHW in 039430 with the SOL	66.66	33.34
LHW in 039430 without the SOL	86.97	13.03
LHW in 039440 with the SOL	59.64	40.36
LHW in 039440 without the SOL	86.01	13.99

The presence of the SOL results in a significant increase in the LH power absorbed via collisions in the SOL. With the SOL included in the simulation, the collisional damping can be comparable to the Landau damping. The LHCD efficiency would be significantly reduced by the power loss in the SOL especially in the discharge 039440 which is an even lower absorption regime for the LHW, and this simulation result is consistent with the experimental observation which shows that more LH power was required in the discharge 039440 to drive the same level of current as that in the discharge 039430. Indeed these results also point to a potential cause for the decline in hard x-ray emission that has been observed in LHCD experiments on EAST **[Ding, 2013]** as the line averaged density is increased above 3 – 3.5 $\times$ 10^{19} m^{-3}; namely the increase in collisional damping of LH waves in the periphery. Proper investigation of this last point however would require simulation of the hard x-ray emissivity using the fast electron distribution from GENRAY-CQL3D in a synthetic diagnostic code for hard x-rays.

To rerun the cases for the two discharges to be compared with experiments quantitatively, the effect of the dc electric field was first included in the simulation by using the experimental level of loop voltage equal to 0.5 V to calculate the total current. Also, the radial transport was turned on in the CQL3D simulation for both discharges with various transport coefficients that are independent of radius and velocity. Quite importantly the experimental value of 1.65 MW of injected LH power was used in the GENRAY simulation for the discharge 039440. The LH current drive and total current drive versus the fast electron diffusion coefficients are shown in Figure 8(a), and it can be seen that when the diffusion coefficient reaches to $0.2\ \mathrm{m}^2/\mathrm{s}$ the values of total driven current in both discharges are close to the experimental value. The profiles of both LH current density and the total current density simulated with $\chi_{\mathrm{F}} = 0.2\mathrm{m}^2/\mathrm{s}$ for the two discharges are shown in Fig. 8(b). The total current (LH + Ohmic) in Fig. 8(b) is 383 kA for the discharge 39430 and 388 kA for the discharge 39440, which are both close to the experimental value ~386kA for both discharges. The integrated LH current without the DC electric field [also shown in Fig. 8(b)] is 142 kA for discharge 39430 (black dashed line) and is 149 kA for

discharge 39440 (red dashed line).

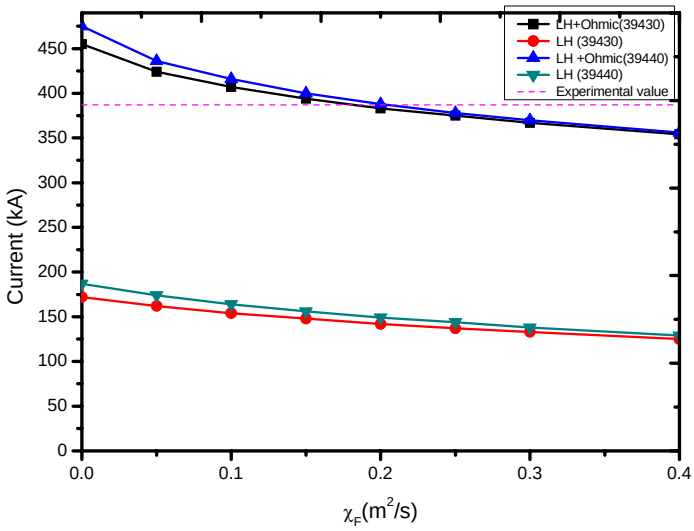

Figure 8(a)

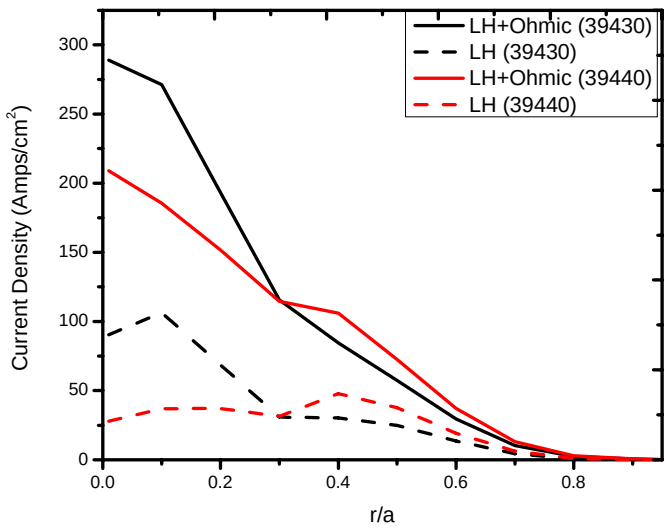

Figure 8(b)

Figure. 8 (a)Integrated LH current and total integrated current versus the fast electron diffusion coefficients. (b) Current density profiles of the LH (black and red dashed curves) and the LH+Ohmic (solid red and black curves) in the two discharges using χ_F = 0.2 m^2/s. The total current (LH + Ohmic) is 383 kA for the discharge 39430 and 388 kA for the discharge 39440. The integrated LH current without the DC electric field is 142 kA for discharge 39430 and is 149 kA for discharge 39440.

The simulation results in Fig.8 indicate that the observed levels of total current are

qualitatively consistent with the fact that almost 40% more LH power is launched in the discharge 039440 to obtain the same amount of current drive as in the discharge 039430. Note these levels of total current are also consistent with the fact that 30-40% of the total injected LH wave power is lost in the SOL via collisions. Furthermore this finding could indicate that one possible explanation for the significant differences in LH power needed to maintain the same total current at the same density and loop voltage in two different discharges may be the sensitivity of the absorption to small variations in plasma conditions (such as the poloidal field profile) when in the weak absorption regime.

Section IV. Full wave simulations of low density EAST case

It can be seen from the simulations in the previous subsections that LH ray trajectories undergo many passes before being absorbed because of the low electron temperatures and weak damping that characterize the EAST target discharges. It is useful therefore to simulate some of these cases using a full-wave electromagnetic field solver where reflections at the plasma edge, wave diffraction, and poloidal mode coupling are all treated more accurately, relative to the geometrical optics approach. It is necessary to mention that the full wave code TORLH still lacks a model for the SOL, so it is not suitable to apply that solver to the modeling of LHCD in EAST discharges with higher density where the collisional damping in the SOL is significant. Also as explained below, the full-wave field solver TORLH was not iterated self-consistently with the Fokker Planck code CQL3D. Instead the final electron distribution function from a quasilinear ray tracing / Fokker Planck iteration was used in the full-wave field solver in order to investigate any differences in the damping profiles that would be due to full-wave effects alone.

Comparisons between the absorbed LH power density from the GENRAY ray tracing code and the TORLH full-wave solver are shown in Figs. 9(a) and 9(b). The parameters used in these simulations are: $\mathrm{n_e}(0) = 1.0 \times 10^{19}\mathrm{m}^{-3}, \mathrm{T_e}(0) =$

$1.5\ \mathrm{keV},\ \mathrm{I_p} = 480\ \mathrm{kA}, \mathrm{f_0} = 2.45\ \mathrm{GHz},\ \text{and}\ \mathrm{n_\parallel}(0) = -2.1.$ The ray tracing code and the Fokker Planck code were iterated to self-consistency as described in Section II-E. The ray tracing calculation used 5×35(35 rays from each of the 5 poloidal positions) rays with a single lobe in the power spectrum around $\mathrm{n_\parallel}(0) = -2.1$ with no radial diffusion operator in the Fokker Planck equation. In the iterated calculation, the ray tracing was recalculated each time the Fokker Planck code is called to advance the distribution function in time (i.e., every 20 msec with 50 time steps.). The integrated powers from ELD in the ray tracing and the Fokker Planck codes are found to agree quite closely (to within a few percent) in steady state. The converged quasilinear distribution function from the Genray / CQL3D iteration was then used once in the TORLH full-wave field solver and the deposition profiles based on the full-wave and ray tracing codes were compared using the same quasilinear distribution function as shown in Fig. 9(b). For comparison, the results for the wave damping in GENRAY and TORLH using a Maxwellian distribution are shown in Fig. 9(a). The differences in GENRAY and TORLH in Figs. 9(a) and 9(b) can therefore be taken as an indication of the relative importance of full-wave effects in these cases since both propagation codes utilized the same electron distribution functions for the damping in each case. The quasilinear damping profiles for full-wave and ray – tracing shown in Fig. 9(b) are qualitatively and even quantitatively similar, with the primary difference being a slight inward shift of the peak in the deposition profile for the full-wave case. In contrast the linear damping profiles shown in Fig. 9(a) differ more qualitatively; both profiles are broad however the ray tracing profile is peaked in the core whereas the full-wave profile is flat and peaked more at the edge. The differences seen for the linear damping comparison in Fig. 9(a) may be due to diffraction effects which tend to spatially spread the wave packet near a caustic, thus resulting in a lower power density relative to the ray tracing **[Wright, 2013]**. These differences do not appear when full-wave and ray tracing are compared for quasilinear damping [see Fig. 9(b)], which may be because the damping occurs farther off-axis. The total profile widths are about the same in each case, although

the profile width from the ray tracing simulation in Fig. 9(a) is somewhat broader, extending farther out to the plasma edge than in the full-wave. It's important to note that, although still challenging for the weak damping cases in the devices with large aspect ratio such as EAST, if we do self-consistent iteration between the full wave solver and the Fokker-Planck code for the quasilinear case, the history of the time evolution of the quasilinear absorption could be different and the agreement shown in Fig. 9(b) might not be obtained.

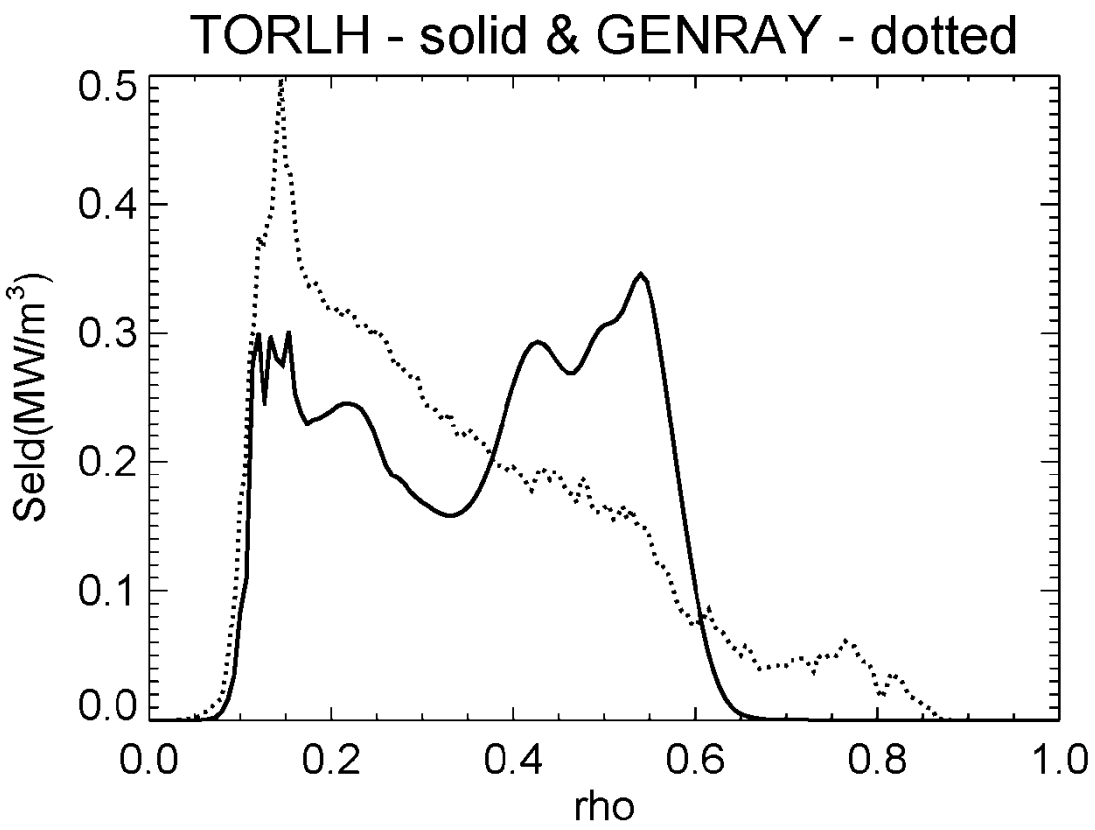

Figure 9(a)

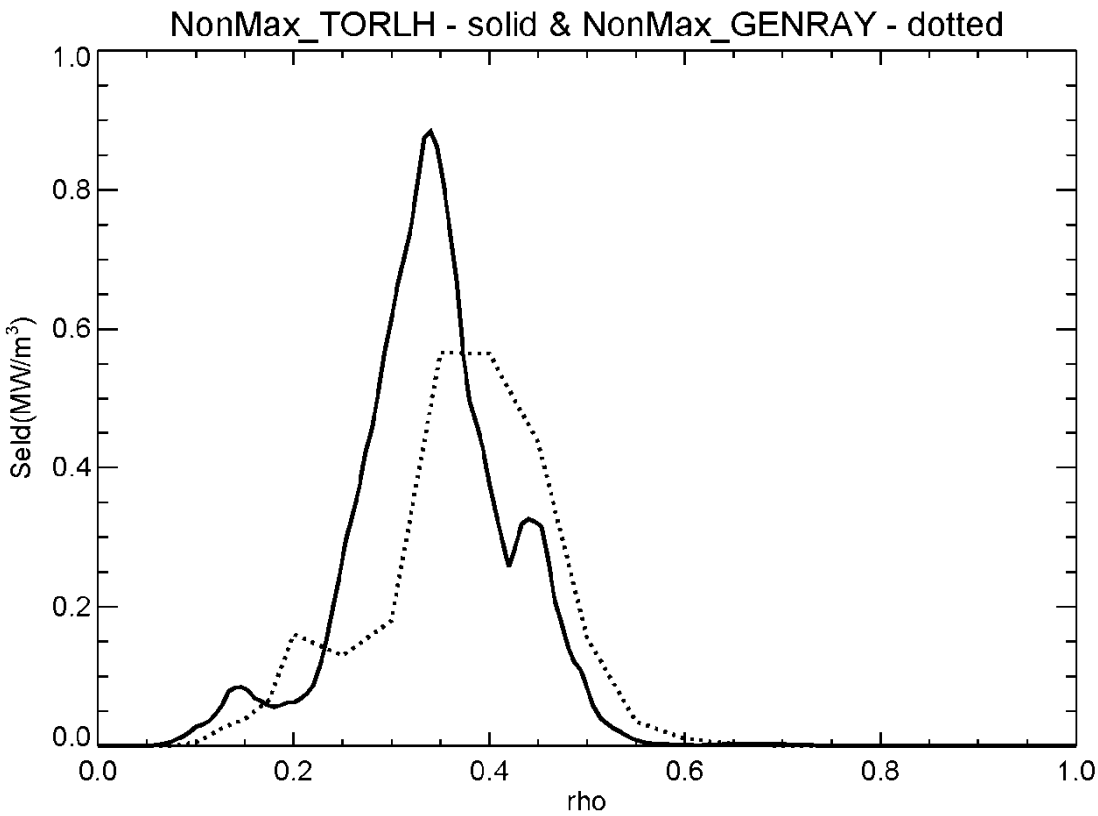

Figure 9(b)

Figure 9: Comparison of GENRAY and TORLH absorption profiles based on (a) Maxwellian electron distribution function and (b) quasilinear electron distribution function from a GENRAY-CQL3D iteration. The solid curve corresponds to TORLH and the dotted curve corresponds to GENRAY. The power absorption is given as (MW/m^3) versus square root of normalized toroidal flux (rho). The integrated LH power in each case is close to 1 MW. The parameters used in these simulations are: $n_e(0) = 1.0 \times 10^{19} m^{-3}, T_e(0) = 1.5\ keV,\ I_p = 480\ kA, f_0 = 2.45\ GHz,$ and $n_{\parallel}(0) = -2.1$

The level of qualitative agreement in the absorption profiles between the full-wave and ray tracing in Figs. 9 provides some confirmation of the ray tracing result within the context of the more complete full-wave treatment. Furthermore, the variations in poloidal mode number and poloidal mode coupling that are predicted by ray tracing to be needed to close the spectral gap between the injected LH waves and tail electrons at $3 \times V_{Te}$ are also found to occur in the full-wave simulations. This is shown in Fig. 10(a) where we plot the fast Fourier transform (FFT) of the $Re(E_\zeta)$ electric field component versus poloidal mode number (m) on a range of flux

surfaces that span the plasma cross-section ($0.1 \leq r/a \leq 1.0$) for the TORLH simulation that used a Maxwellian distribution for the electrons. The right side shows a sharp drop off corresponding to local wave accessibility in the plasma. The left side, on the other hand, shows that significant spectral power cascades via poloidal mode coupling to values of $|m| \geq 500$, corresponding to values of the parallel refractive index that are 2-3 times the initial value of 2.1 which gives rise to sufficient Landau damping. For the outer flux surfaces, at the endpoints ($|m| \approx$ 700-1000) of the spectra the m-spectrum values are at least two orders of magnitude below those near m=0, which provides evidence that the spectral expansion is converged throughout the plasma with 2047 poloidal modes. As shown in Fig.10(b), the spectral plots for the TORLH simulation using the converged quasilinear distribution function [Fig. 9(b)] also exhibit similar cascading of power via poloidal mode coupling.

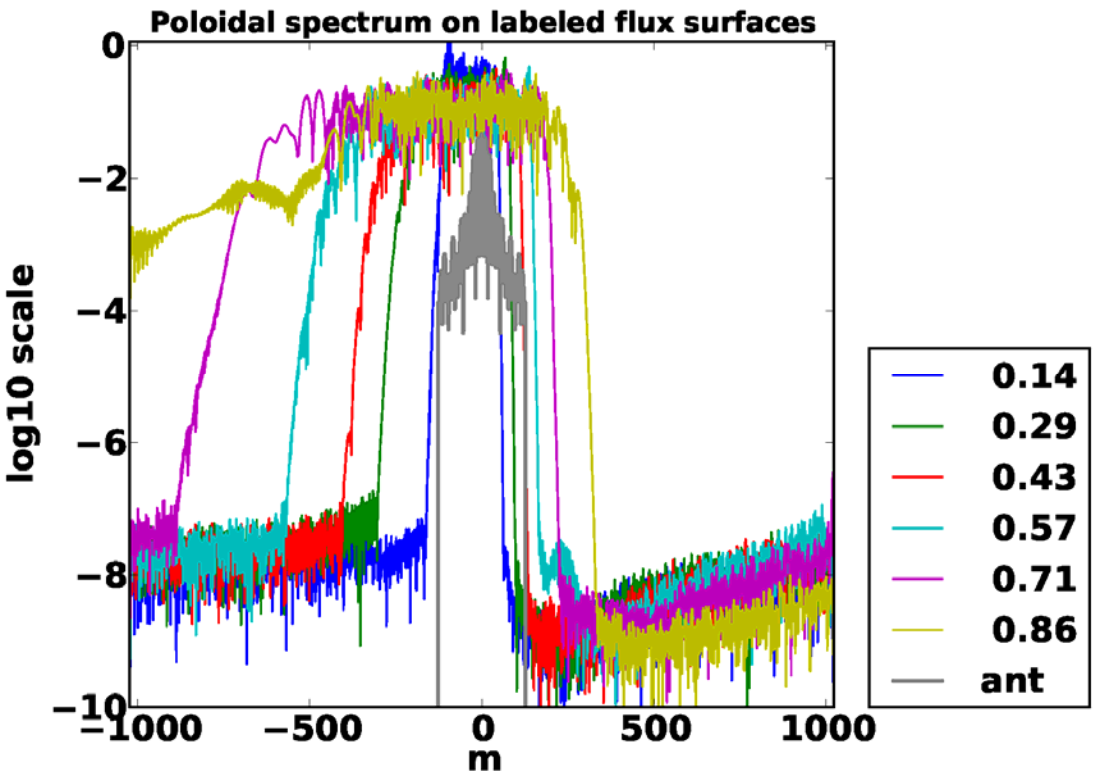

Fig. 10(a)

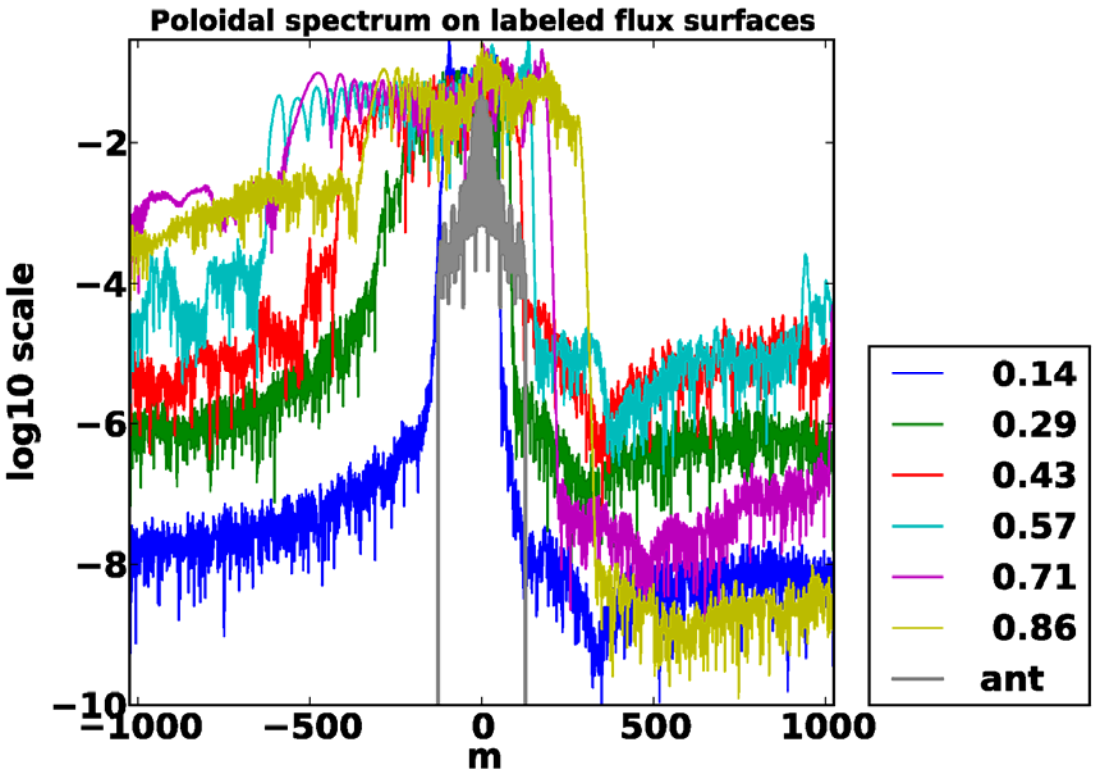

Fig. 10(b)

Figure 10: Fast Fourier transform (FFT) of the Re(E_ζ) electric field component versus poloidal mode number (m) on flux surfaces at r/a =(0.14, 0.29, 0.43, 0.57, 0.71, 0.86, 1.0) for the TORLH simulation (a) with a Maxwellian electron distribution function and (b) using the converged quasilinear distribution function.

Finally contour plots of the Re(E_ζ) electric field component are shown in Figure 11 corresponding to the TORLH simulation based on Maxwellian Landau damping [Fig. 11 (a)] and based on the quasilinear electron Landau damping [Fig. 11(b)]. The full-wave fields in 11(a) tend to fill more of the poloidal cross-section than the field pattern shown in 11(b). This makes sense physically in that the simulation in 11(a) is based on a Maxwellian distribution where the damping is weaker because no quasilinear plateau has yet formed. When the distribution function from GENRAY-CQL3D is used that has the fully developed plateau, the damping is stronger and the fields tend to damp with fewer passes of the wave front as shown in Fig. 11(b). Both field patterns from the TORLH simulations exhibit a cusp-shaped

reflection from the top of the poloidal cross-section where the field intensity is high. This feature is also seen in the ray tracing and represents a reflection point from the plasma edge from which large increases in the parallel wavenumber occur through a combination of toroidicity and poloidal field **[P. T. Bonoli, 1982]**. The subsequent damping of the wave field that accompanies this upshift is evident in the full-wave simulation where the field amplitude rapidly decays as the wavefront propagates into the plasma core.

(a) Maxwellian electron Landau damping	(b) Quasilinear electron Landau damping
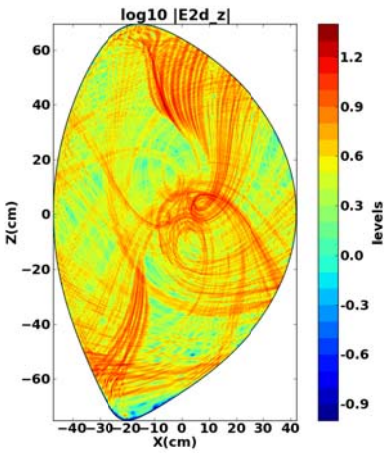	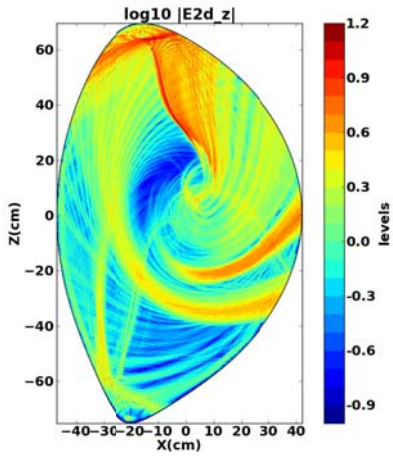

Figure 11: TORLH simulations of low density EAST discharge [$n_e(0) = 1.0 \times 10^{19}$ m^{-3}, $T_e(0) = 1.5$ keV, and $I_p = 480$ kA, $f_0 = 2.45$ GHz, and $n_{//}(0) = 2.1$] using (a) Maxwellian electron damping and (b) quasilinear electron Landau damping. Shown are the contours of the Re(E_ζ) electric field component.

Section Ⅴ Discussions and conclusions

Using the GENRAY-CQL3D codes, the LHW physics and LHCD in weak absorption regimes characterized by low electron temperature and large spectral gap has been modeled and studied for EAST. It was found that despite the higher aspect ratio in EAST (A ~ 4) relative to other present day tokamaks (A ~ 3) that large toroidally induced increases in the parallel wavenumber still occur, confirming that LH ray trajectories in EAST can be characterized by stochastic phase behavior [Bonoli, 1982].

A low density case was modeled first. The simulated power deposition profiles were found to be peaked off-axis despite excellent wave accessibility to the plasma center. This is because the LH power deposited via Landau damping relies on the up-shift of $n_{\|}$ in the low temperature (1.5 keV) case. This upshift occurs after reflection of the wavefront from the plasma edge or cut-off, near the bottom of the poloidal cross-section. As the wave propagates inward, the increase in poloidal mode number is rapidly converted through the poloidal field to a large increase in $\mathrm{n}_{\|}$ that satisfies the conditions for strong electron Landau damping before the wave reaches the center of the plasma.

Lower hybrid current drive calculated by CQL3D without radial diffusion is overestimated in comparison with the experiment. When collisional losses in the SOL and radial diffusion with a fast electron diffusivity in the range of $0.25 - 0.3\ \mathrm{m}^2/\mathrm{s}$ are included in the simulation, the LHCD calculated for a steady state discharge with zero loop voltage is close to the one from experiment. In order to confirm the importance of fast electron and collisional losses in EAST it is ultimately necessary to carry out detailed comparisons between simulated and measured diagnostic data for hard x-ray emission and electron cyclotron emission (for example).

Ray accessibility in a higher density ($4.0 \times 10^{19}\ \mathrm{m}^{-3}$ and $\mathrm{B}_0 \sim 2\mathrm{T}$) case was also studied. For the EAST LH system with 2.45 GHz frequency and $\mathrm{n}_{\|} \sim 2.1$, the ray was not able to penetrate into the plasma center initially but did access the core after multiple reflections from the plasma edge which result in sufficient up-shift of $\mathrm{n}_{\|}$. This loss of wave accessibility in EAST discharges at line averaged densities of 3 - 4 $\times$ 10^{19} m^{-3} combined with collisional damping losses could be playing a role in the rapid decline in hard x-ray emission that has been observed in LHCD experiments on EAST at these densities [Ding, 2013].

The LHW physics in EAST with a SOL in higher density cases has also been modeled. Lower hybrid current drive in two discharges with identical current, magnetic field, density, and loop voltage, yet significantly different LHRF powers were studied and compared. The results indicate that the power deposited in the SOL through collisions can be comparable with electron Landau damping resulting in a significant reduction in LHCD efficiency, especially in the weak absorption case. It was further found through simulation that the LH rays tended to damp after only a few passes in the discharge where less LH power (1.2 MW) was required to sustain the current through a combination of Ohmic drive and LH drive assisted by the DC electric field effect. In contrast the discharge where more LH power (1.65 MW) was required to sustain the combined ohmic and non-inductive current, more passes of the LH rays occurred before the wave was damped. It was shown that these differences in the wave behavior could be attributed to differences in the poloidal magnetic field profile, despite the total current being the same in both cases, which is consistent with the ray behavior being sensitive to plasma configuration in the weak damping regime.

Finally in Section IV a low density EAST discharge was simulated using the TORLH full-wave field solver and the results were compared with a ray tracing – Fokker Planck calculation from GENRAY-CQL3D. The full-wave field solver was run with both a Maxwellian electron distribution function (linear damping) and with the quasilinear distribution from an iterated GENRAY-CQL3D calculation. The spatial profiles of the quasilinear electron Landau damping were found to be qualitatively similar, with the primary differences being in the location of the profile peaks. However, in the linear case, the full wave solver gives a flatter profile with the power deposition peaked farther out as compared with ray-tracing, and this may be due to the diffraction effects. The poloidal mode coupling and subsequent up-shifts in the parallel wavenumber in the ray tracing and full-wave were also found to be comparable, thus giving some confidence in the result that toroidally induced increases in the parallel wavenumber may be at least partially responsible for closing the LHCD spectral gap

in low density EAST discharges with LHCD. It is important to note however that the ray tracing simulations at low density ($\sim 1 - 1.5 \times 10^{19}\ \mathrm{m}^{-3}$) exhibit minimal collisional absorption of the LH power in the plasma periphery and scrape off layer (SOL). An accurate model of the SOL geometry, density, and temperature profiles is not as yet available in the TORLH solver. Thus, if the full-wave simulations were performed at higher density where collisional absorption is more important it would be necessary to use a solver which does have such a capability such as the LHEAF code **[S. Shiraiwa, 2011]**. Then it would be possible to compare full-wave and ray tracing simulations for the EAST discharges in Section III. In the future it would also be important to perform iterated simulations using the field solver and a Fokker Planck code in order to capture important interference effects in the RF diffusion coefficient that have been shown to be important in weak damping regimes [Wright, 2014].

In conclusion, we have used a combined ray tracing / Fokker Planck model (GENRAY-CQL3D) and a full-wave field solver (TORLH) to interpret LHCD experiments characterized by weak absorption of the LH waves in the EAST tokamak. Loss of wave accessibility, collisional damping of LH waves in the SOL, and spatial diffusion of fast electrons were all identified as important physics mechanisms that must be accounted for in order to understand these experiments.

Acknowledgements

The authors would like to thank the members of EAST Team for their cooperation and kind help. This work was supported in part by US Department of Energy Contract Numbers DE-FC02-01ER54648-Sci-DAC and DE-FC02-99ER54512 and in part by National Natural Science Foundation of China under Grant No. 11105178. Computer simulations using GENRAY, CQL3D and TORLH were carried out on the MIT PSFC parallel AMD Opteron/Infiniband cluster Loki and the high performance computing cluster ShenMa at IPP CAS.

References

[Andrews, 1983] P. L. Andrews and F. W. Perkins Physics of Fluids 26, 2537 (1983)

[Baranov, 1996] Yu. F. Baranov et al., Nuclear Fusion 36, 1031 (1996)

[Barbato, 2011] E. Barbato, Nuclear Fusion 51, 103032 (2011)

[Bertelli, 2013] N. Bertelli, G. Wallace, P. T. Bonoli et al, Plasma Physics and Controlled Fusion 55, 074003(2013)

[Bizarro and Moreau, 1993] J. P. Bizarro and D. Moreau, Phys. Fluids B 5, 1227 (1993)

[Bizarro, 1993]J. P. Bizarro, Nucl. Fusion 33, 831 (1993)

[Bizarro, 1995] J. P. Bizarro et al., Physical Review Letters 75, p. 1308 (1995)

[Bizarro, 1999] J. P. Bizarro, J. S. Ferreira and R. Nakach, Physics of Plasmas 6, p. 1131 (1999)

[Bizarro, 2010] J. P. S. Bizarro, Physics of Plasmas 17,104501 (2010)

[Bonoli, 1981] P. T. Bonoli and E. Ott, Physical Review Letters 46, 424 (1981)

[Bonoli, 1982] P. T. Bonoli and E. Ott, The Physics of Fluids 25, 359 (1982)

[Bonoli, 1984] P.T Bonoli, IEEE Trans, Plasma Sci. 12, 95(1984)

[Bonoli, 1986] P. T. Bonoli and R. C. Englade, Phys. Fluids 29, 2937 (1986)

[Bonoli, 1990] P. T. Bonoli et al., Nuclear Fusion 30, 533 (1990)

[Brambilla, 1976] M. Brambilla, Nuclear Fusion 16, 47 (1976)

[Brambilla, 1979] M. Brambilla, Nuclear Fusion 19, 1343 (1979).

[Cesario, 2004] R. Cesario, A. Cardinali, C. Castaldo, F. Paolletti, D. Mazon, and the EFDA JET Contributors, Physical Review Letters 92, 175002 (2004)

[Cesario, 2010] R. Cesario, L. Amicucci, A. Cardinali et al, Nature Communications, DOI: 10.1038/ncomms1052 (2010)

[Decker, 2004] J. Decker and Y. Peysson, "DKE: A fast numerical solver for the 3D drift kinetic equation", Euratom-CEA Report, EUR-CEA-FC-1736 (2004)

[Decker, 2011] J. Decker, Y. Peysson, J.-F. Artaud et al, in Radiofrequency Power in Plasmas, AIP Conference Proceedings 1406 (AIP, NY 2011), Eds. C K. Phillips and J. R. Wilson, pp. 447-450

[Decker, 2014] J. Decker, Y. Peysson, J.-F. Artaud, E. Nilsson, A. Ekedahl, M. Goniche, J. Hillairet, D. Mazon, 20th Topical Conference on Radio Frequency Power in

Plasmas, AIP Conference Proceedings 1580, Eds. A. Tuccillo and S. Ceccuzzi (AIP, NY, 2014).

[Devoto, 1992] R. S. Devoto et al., Nuclear Fusion 32, 773 (1992)

[Ding, 2011] B. J. Ding, Y. L. Qin, W. K. Li, et al. Physics of Plasmas 18, 082510 (2011)

[Ding, 2013] B. Ding, E. H. Kong, M. Li, et al, Nuclear Fusion 53, 113027 (2013)

[Fuchs, 1989] Fuchs et al. Nucl. Fusion 29, p. 1479 (1989)

[Gao, 2010] Xiang Gao, Yao Yang, Zixi Liu, Long Zeng, Shoubiao Zhang, Nan Shi, Yinxian Jie, Wei Liao, Yumin Wang, Jingliang Bu, Baonian Wan, Jiangang Li, and the EAST Team, "Experimental Study of Plasma Confinement on EAST", 23rd IAEA Fsuion Energy Conference (Daejon, 2010), Paper IAEA-F1-CN-180- EXC/P4-06.

[Harvey, 1992] R. W. Harvey and M. McCoy, in Proceedings of the IAEA Technical Committee Meeting on Simulation and Modeling of Thermonuclear Plasmas,Montreal, Canada, 1992 (IAEA, Vienna, 1992), USDOC NTIS Document No. DE93002962

[Ignat, 1981] D. W. Ignat, Phys. Fluids 24, p. 1110 (1981)

[Jones, 1993] S. Jones, S. von Goeler, S. Bernabei, et al., Plasma Physics and Controlled Fusion 35, 1003 (1993)

[Kerbel, 1985] G. D. Kerbel and M. G. McCoy, Phys. Fluids 28, 3629 (1985)

[Kupfer, 1993] K. Kupfer, D. Moreau, X. Litaudon, Physics of Fluids B 5, p. 4391 (1993)

[Lao, 1985] L.L. Lao et al., Nuclear Fusion 25 1421 (1985)

[Meneghini, 2009] O. Meneghini et al, Physics of Plasmas 16, 090701 (2009)

[Meneghini, 2012] O. Meneghini, "Full-wave modeling of lower hybrid waves on Alcator C-Mod", PhD Dissertation, Nuclear Engineering and Science Department, MIT (2012)

[Mynick, 1980] H. E. Mynick and J. A. Krommes, Physics of Fluids 23, 1229 (1980)

[Mynick, 1981] H. E. Mynick and J. D. Strachan, Physics of Fluids 24, 695 (1981)

[Naito, 2002] O. Naito et al., Physical Review Letters 89, 065001 (2002)

[Peysson, 1993] Y. Peysson, Plasma Physics and Controlled Fusion 35, B253 (1993)

[Peysson, 1996] Y. Peysson, R. Arslanbekov, V. Basiuk, J. Carrasco, X. Litaudon, D.

Moreau, and J. P. Bizarro, Physics of Plasmas 3, 3668 (1996)

[Peysson, 2000] Y. Peysson et al., Plasma Physics and Controlled Fusion 42, B87 (2000)

[Peysson, 2011] Y. Peysson, J. Decker, L. Morini, and S. Coda, Plasma Physics and Controlled Fusion 53, 124028 (2011)

[Peysson, 2012] Y. Peysson, J. Decker, and L. Morini, Plasma Physics and Controlled Fusion, 54, 045003 (2012)

[Pereverzev, 1992] Pereverzev et al., Nuclear Fusion 32, p.1091 (1992)

[Rax, 1989] Rax, Moreau, Nuclear. Fusion 29, p. 1751 (1989)

[Rechester, 1978] A. B. Rechester and M. N. Rosenbluth, Physical Review Letters 40, 38 (1978)

[Schmidt, 2011] A. Schmidt, P. T. Bonoli, O. Meneghini et al., The Physics of Plasmas 18, 056122 (2011)

[Shi, 2011] Yuejiang Shi et al, PRL 106, 235001 (2011)

[Shiraiwa, 2011] S. Shiraiwa, J. Ko, O. Meneghini et al, The Physics of Plasmas 18, 080705 (2011)

[Smirnov,1995] A. P. Smirnov and R. W. Harvey, Bull. Am. Phys. Soc. 40, 1837, (1995)

[Troyon, 1974] F. Troyon, F. and F. W. Perkins, "Lower-hybrid heating in large tokamak", Proceedings of the Second Topical Conference on Radiofrequency Plasma Heating (Texas Tech University, Lubbock, Texas, 1974) Paper B4

[Wallace, 2010] G. M. Wallace, R. R. Parker, P. T. Bonoli et al., The Physics of Plasmas 17, 082508 (2010)

[Wan, 2009] B. N. Wan et al., Nucl. Fusion 49, 104011 (2009)

[Wang, 2012] L. Wang, G.S. Xu, H.Y. Guo Nucl. Fusion 52 063024(2012)

[Wright, 2009] J. C. Wright, P. T. Bonoli, A. E. Schmidt et al, The Physics of Plasmas 16, 072502 (2009)

[Wright, 2013]J. C. Wright and N. Bertelli, "The effect of finite electron temperature and diffraction on lower hybrid waves", submitted to Plasma Physics and Controlled Fusion, 2013

[Wright, 2014] J. C. Wright A. Bader, L. A. Beryy et al, Plasma Physics and Con. Fusion 56 045007 (2014)